Chemical Geology 615 (2023) 121196

Contents lists available at ScienceDirect

Chemical Geology

journal homepage: www.elsevier.com/locate/chemgeo

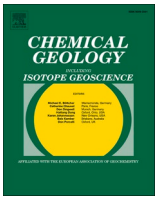

Formation of Paleo- to Meso-Archean continental crust in the western Dharwar Craton, India: Constraints from U—Pb zircon ages and Hf-Pb-Sr isotopes of granitoids and sedimentary rocks

Arathy Ravindran [a,b,*], Klaus Mezger [a], S. Balakrishnan [c], Jasper Berndt [d], Sameer Ranjan [e,f], Dewashish Upadhyay [e]

[a] Institut für Geologie, Universität Bern, Baltzerstrasse 1+3, 3012 Bern, Switzerland
[b] Institut für Geochemie und Petrologie, ETH Zürich, Clausiusstrasse 25, 8092 Zürich, Switzerland
[c] Department of Earth Sciences, Pondicherry University, Puducherry 605014, India
[d] Institut für Mineralogie, Universität Münster, Corrensstrasse 24, 48149 Münster, Germany
[e] Department of Geology and Geophysics, IIT Kharagpur, West Bengal 721302, India
[f] Geochemistry Division, National Geophysical Research Institute, Telengana 500007, India

ARTICLE INFO

Editor: S Aulbach

Keywords:
Archean granitoids
Crust-mantle evolution
Hf-Sr-Pb isotopes
U-Pb zircon ages
Dharwar Craton
Crustal growth

ABSTRACT

The combination of U—Pb zircon ages with Hf-Sr-Pb isotopes of different intrusive and extrusive felsic and sedimentary rocks provides constraints on the petrogenetic evolution of the continental crust in the western Dharwar Craton, India. The oldest detrital zircon preserved formed at ~3.6 Ga and represents a relic of the oldest felsic crustal material in the region. The dominant granitoid units of the western Dharwar Craton contain zircon grains with magmatic ages between 3.4 Ga and 3.0 Ga that indicate the formation of major felsic continental crust during this interval.

Trace element abundances of the granitoids indicate that the oldest members of the intermediate to felsic suite derived by partial melting of mafic material at ~3.6–3.4 Ga. The initial bulk rock Hf isotope compositions of these granitoids are consistent with their formation by melting of even older mafic material that was slightly enriched relative to the depleted mantle composition. This mafic and slightly enriched material formed by mantle melting at ~ < 3.8 Ga. The Hf isotope compositions of individual zircon grains, obtained by two different analytical techniques (in-situ and complete dissolution followed by chromatographic separation) give evidence for the presence of such older mafic material (<3.8 Ga) that formed the immediate precursor of their granitoid host rocks. Such a mafic source for the granitoids is consistent with Pb—Sr isotope systematics of these that shows no indication of Eoarchean enriched/evolved material in the western Dharwar Craton. The mafic source material of the granitoids thus represents an intermediate stage of crust formation that started after 3.8 Ga with the formation of mafic crust by mantle melting. The combined geochronological and isotopic constraints suggest that the Mesoarchean felsic crust of the Dharwar Craton formed by differentiation of melts derived from an amphibolite/eclogite source rock and included increasing contributions of reprocessed crustal material with time from ~3.6 to 3.0 Ga. The major interval of growth of felsic continental crust was from 3.4 to 3.0 Ga. The younger generation of granitoids formed mostly by reworking of older intermediate to felsic crust. These different felsic magmatic bodies with distinct petrogeneses and sources, that include the depleted mantle, older mafic crust and the evolved continental crust, became essential elements of the stable continental crust of the western Dharwar Craton, the majority of which was generated from 3.4 to 3.0 Ga.

1. Introduction

A typical feature of the Earth as a planet is its distinct continental crust. It is generally accepted that this crust was generated over time, by magmatic differentiation of material originally derived as basaltic melt from the mantle (e.g., Armstrong, 1991; Taylor and McLennan, 1985).

* Corresponding author at: Institut für Geologie, Universität Bern, Baltzerstrasse 1+3, 3012 Bern, Switzerland.
E-mail address: arathy.ravindran@geo.unibe.ch (A. Ravindran).

https://doi.org/10.1016/j.chemgeo.2022.121196
Received 11 September 2022; Received in revised form 30 October 2022; Accepted 31 October 2022
Available online 4 November 2022

The nature of this ancient thick and felsic crust, its petrogenesis and the timing of its formation have been the focus of many recent integrated studies using different geochemical parameters including major and trace elemental abundances as well as stable and radiogenic isotope compositions (e.g., Belousova et al., 2010; Dhuime et al., 2015; Smit and Mezger, 2017). Of major interest are the possible differentiation processes that led to the formation of felsic crust from ultramafic mantle material (e.g., Bauer et al., 2017; Kemp et al., 2010; Reimink et al., 2020). The study of the petrogenetic processes using isotope compositions and element abundances in the preserved rock records is somewhat hampered by post-emplacement metamorphic overprinting which has been identified in all Archean igneous and sedimentary rocks (e.g., Lahaye et al., 1995; Moorbath et al., 1997). Hence, crustal rocks that are exposed and that preserve their primary radiogenic isotope signatures for all elements are rare in the Hadean-Archean rock record, making it a challenge to reconstruct their petrogenesis. The mineral zircon plays a key role in these studies because it gives the most reliable and precise ages for (felsic) crust formation and modification due to its robustness towards alteration and re-equilibration (e.g., Mezger and Krogstad, 1997). It also yields reliable initial Hf isotope ratios (e.g., Amelin et al., 2000) even in rocks with complex thermal histories (e.g., Gerdes and Zeh, 2009; Guitreau et al., 2019). Thus, zircon and its Hf isotopic composition can constrain the source of the material, and at the same time, provide temporal markers for its geochemical evolution. Using zircon, it has been demonstrated that most ancient rocks record a multi-episodic and polymetamorphic history (e.g., Iizuka et al., 2007; Reimink et al., 2014; Guitreau et al., 2012) attesting to a complex history from melting of the mantle to the establishment of evolved, stable continental crust on early Earth. Considering these complexities different models for the amount and extent of early continental crust have been suggested but they remain to be quantified on a global scale.

Radio-isotope systems such as Lu—Hf, Sm—Nd, Rb—Sr, *Re*—Os and Pb—Pb can be used to quantify the evolution of continental crust on the early Earth, as well as its composition, as all these systems are sensitive to different degrees to crust as well as mantle differentiation. These isotope systems, along with proper understanding of petrogenetic processes, can provide key information on the time and extent of early mantle differentiation that is related to the formation and growth of felsic continental crust. They can be used to identify chemical differentiation processes and provide information on the timing of these processes, but they cannot describe the style of tectonic activity that led to the formation of crustal rocks (e.g., Laurent and Zeh, 2015). However, certain isotopes, e.g., Hf—O, are not always suitable to place unique constraints on crustal growth (Couzinié et al., 2016). Most of the radio-isotope systems, especially the Rb—Sr and to a lesser extent the Sm—Nd and Lu—Hf systems, are prone to alteration by metamorphism, which can lead to the retrieval of wrong initial isotope ratios for the host rock (Moorbath et al., 1997; Fisher et al., 2020; Hammerli et al., 2019; Ravindran et al., 2020). Zircon can be formed and altered during multiple magmatic and metamorphic episodes, with serious consequences for the interpretation of combined U—Pb and Lu—Hf isotopic data obtained by in-situ laser analyses (e.g., Gerdes and Zeh, 2009). Therefore, Archean rocks that have their primary geochemical and isotopic compositions preserved or for which these parameters can be confidently reconstructed are important for evaluation of early crustal evolution. Among the Archean rocks, the widespread tonalite-trondhjemite-granodiorite (TTG) gneisses are characteristic of early continental crustal material due to their unique composition and formation as derivatives of older mafic rocks (Moyen and Martin, 2012). Hence, geochemical and isotopic signatures of these granitoid rocks can be used to constrain the timing of continental crust formation and the extent of early crust-mantle differentiation.

The Indian shield hosts some of the oldest cratonic nuclei that preserve chemical and isotopic information on early crust-mantle evolution. The western Dharwar Craton in southern India exposes a diverse geological association of Paleoarchean to Mesoarchean rocks including TTG and other granitoid intrusions that date back to at least ~3.4 Ga (Guitreau et al., 2017; Jayananda et al., 2015). This study combines whole rock major-trace element, Rb—Sr and Lu—Hf isotope data, as well as common Pb isotopes of leached feldspar from TTGs with U—Pb ages and Hf isotope compositions of zircon (both in-situ and bulk dissolution) to reconstruct the genesis and evolution of the mostly felsic continental crust of the Dharwar Craton.

2. Geological background

The Dharwar Craton (Fig. 1) is among the largest preserved Archean cratonic nuclei in the world and is one of the oldest cratonic blocks on the Indian subcontinent. It is divided into two major units: the older western Dharwar Craton (Fig. 1, in-set) and the younger eastern Dharwar Craton (Gupta et al., 2003; Swami Nath and Ramakrishnan, 1981) based on the age of rocks, metamorphic grade, crustal thickness and the characteristics of its greenstone belts. Recent studies have also considered a three-fold division of the craton, including an additional Central Dharwar Province (Jayananda et al., 2018). The two cratonic blocks have undergone different magmatic and metamorphic events in the late Archean (Chardon et al., 2011; Jayananda et al., 2013).

The western Dharwar Craton is sub-divided into the older Sargur and younger Dharwar (super) groups. The Sargur Group, in the southern part of the craton forms linear supracrustal belts that expose komatiitic (komatiites and komatiitic basalts) and tholeiitic rocks associated with pelites, carbonates and quartzites (Fig. 1) that are significantly deformed. Mafic and ultramafic whole rock samples from this belt yielded Sm—Nd isochron ages of 3.35–3.10 Ga (e.g., Jayananda et al., 2008; Maya et al., 2017). Contemporaneous TTGs are mostly found associated with the Sargur Group in the Holenarsipur region (Naqvi et al., 2009). The rocks show metamorphic mineral assemblages indicating they reached greenschist to amphibolite facies conditions.

The Sargur Group is unconformably overlain by the 2.9–2.5 Ga Dharwar supergroup (Swami Nath and Ramakrishnan, 1981), which consists of the Bababudan greenstone belt (~3.0–2.9 Ga; Kumar et al., 1996; Ravindran et al., 2021), the Chitradurga greenstone belt (~2.7 Ga; Jayananda et al., 2013) and the younger Shimoga and Gadag greenstone belts. The Shimoga Group lies to the west of the Chitradurga Group and consists of ~2.6 Ga igneous rocks (Nutman et al., 1996).

2.1. Holenarsipur region

Granitoids and sedimentary rocks in the Holenarsipur region (Fig. 1) in the southern part of the western Dharwar Craton constitute one of the oldest parts of the craton. Tonalite-trondhjemite-granodiorite (TTG) gneisses in the Gorur region cover the basement with the oldest ages of ~3.4 Ga (Guitreau et al., 2017; Jayananda et al., 2015; Maibam et al., 2016; Ranjan et al., 2020). Felsic volcanic flows from this region yielded a magmatic zircon U—Pb age of ~3.3 Ga (Peucat et al., 1995). Uranium-Pb zircon ages and Sm—Nd whole rock isochron ages of ~3.24–3.20 Ga were obtained for the anorthosites in the southern part of the belt (Bhaskar Rao et al., 2000; Panicker et al., 2021). Sedimentary rocks in the belt include quartzites, conglomerates, pelites and banded iron formations. Detrital zircons from pelites and quartzites have U—Pb ages as old as ~3.6 Ga (Lancaster et al., 2015; Nutman et al., 1992). Trondhjemite plutons, known locally as the 'Halekote diapiric trondhjemite' (Monrad, 1983) and exposed adjacent to the Gorur gneisses, have U—Pb zircon ages of ~3.2 Ga (Jayananda et al., 2015). Inherited zircon grains as old as 3.6–3.5 Ga have also been reported (Guitreau et al., 2017).

2.2. Bababudan and Shimoga regions

The Bababudan schist belt, belonging to the Dharwar Supergroup, hosts granitoid rocks in the Chikmagalur area that are younger than in the Gorur region (Fig. 1). The Chikmagalur gneisses and granites are

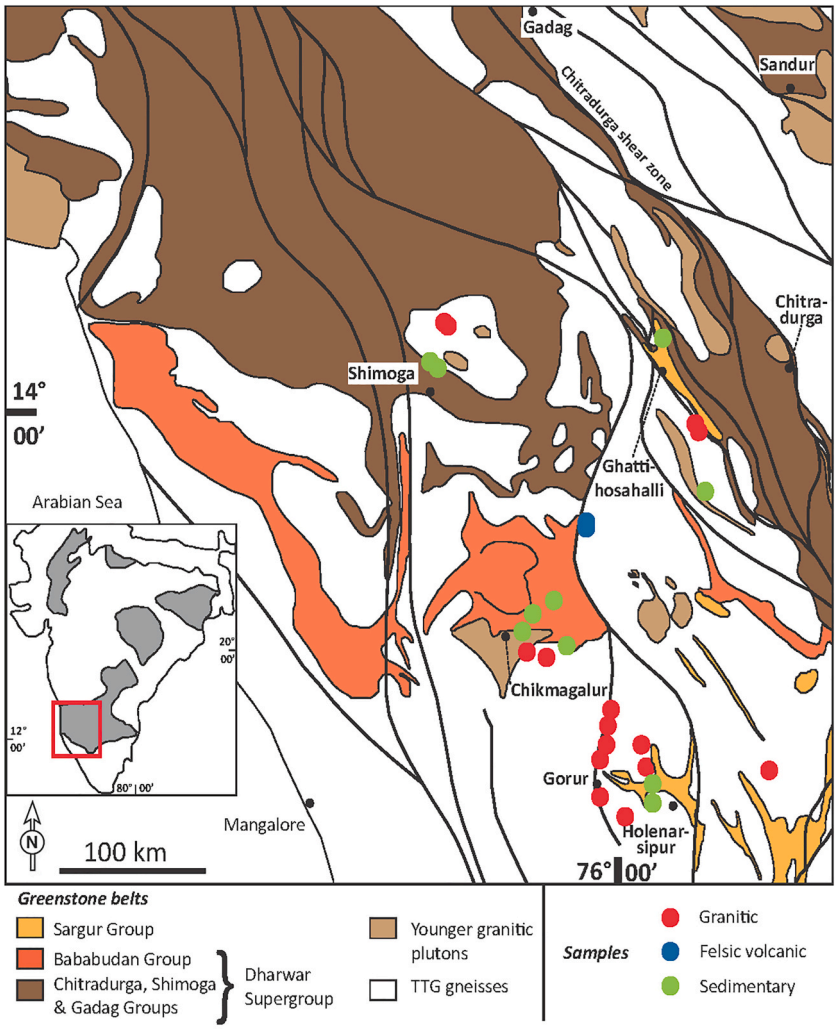

Fig. 1. Geological map of the western Dharwar Craton (modified after Jayananda et al., 2018). The in-set shows a map of India with the Archean cratons of the Indian subcontinent (grey areas). The western Dharwar Craton is marked by a red box. (For interpretation of the references to colour in this figure legend, the reader is referred to the web version of this article.)

~3.3–3.1 Ga old (Jayananda et al., 2015; Taylor et al., 1984); detrital zircon grains from sedimentary rocks in this area are up to ~3.2 Ga old (Hokada et al., 2013). The Honnali dome adjacent to the Shimoga schist belt hosts gneissic and granitic rocks which have not been dated by U—Pb measurements of magmatic zircons.

2.3. Ghattihosahalli region

The Ghattihosahalli schist belt (Fig. 1) is contemporaneous with the Holenarsipur schist belt (~3.2 Ga; Taylor et al., 1984). The adjacent Hosdurga and Chitradurga granites are ~2.6 Ga old (Jayananda et al., 2006; Taylor et al., 1984). Detrital zircon grains in greywackes from the Gadag schist belt gave U—Pb ages of ~3.5 Ga (Sarma et al., 2012). Data on U—Pb magmatic zircon ages of granitoids from the Ghattihosahalli region have not been published so far.

3. Methods of study

The granitoid and sedimentary rocks were collected from the Holenarsipur, Ghattihosahalli, Bababudan and Shimoga greenstone belts and their surrounding meta-igneous rocks in the western Dharwar Craton (Table A1; Appendix A). Most of the gneisses were collected from quarries and fresh outcrops in the Gorur region (Fig.B1(a); Appendix B). The felsic volcanic rocks were collected from a location near Tarikere on the way to Shimoga (Table A1; Appendix A) and were used for U—Pb dating of zircon. Table A1 (Appendix A) presents detailed information on the rock samples that were used for this study, rock type, area of collection and the type of analyses carried out. All granitoids and felsic volcanic rocks have quartz, plagioclase, K-feldspar, biotite, accessory zircon, apatite, titanite and opaque minerals (Fig. B1(b); Appendix B).

3.1. Measurements of major and trace elements

All rock samples were crushed using a steel jaw crusher and a fraction of the crusted sample was powdered using an agate disc mill. Aliquots of 5 g from each powdered sample were analysed at ACTLABS, Canada, for major and trace element concentrations. The samples were mixed with a flux of lithium metaborate and lithium tetraborate and fused in an induction furnace. The molten material was poured into a solution of 5% HNO_3 containing an internal standard and mixed continuously until complete dissolution. All major elements (as oxides) and trace elements such as Sc, V, Sr, Zr, and Ba were analysed on an Agilent 700 Series Inductively Coupled Plasma Optical Emission Spectrometer (ICP-OES). Selected trace and rare earth elements were analysed on a Perkin Elmer SCIEX™ ELAN® 6000 Inductively Coupled Plasma Mass Spectrometer (ICP-MS). Three blanks and five controls

(three before and two after each sample group) were analysed (Table A2; Appendix A). The analytical blanks were below the detection limit for all elements.

3.2. Uranium-Pb zircon dating

The granitoids and felsic volcanic rocks host magmatic zircon, and the sediment samples host detrital zircon grains that were used for U—Pb dating after careful separation. For the separation of zircon grains, a fraction of the crushed samples was sieved (<250 μm) and subjected to magnetic separation after which the preferred fraction was taken for heavy mineral separation. The heavy minerals were separated first on a Wilfley table followed by a density separation with methylene iodide. The zircon grains were hand-picked under a binocular microscope. The mounted and polished zircon grains were examined under secondary electron microscope (for cathodoluminescence and back-scattered electron images) and the ones with oscillatory zoning patterns were chosen for U—Pb dating (Fig.B2; Appendix B). Uranium-Pb measurements were done by laser ablation inductively coupled plasma mass spectrometry (LA-ICPMS) using a ThermoFisher Element2 mass spectrometer coupled to a Photon Machines Analyte G2 Excimer laser at the Institut für Mineralogie, Universität Münster, Germany (Kooijman et al., 2012). Zircon GJ-1 (Jackson et al., 2004) was used for external calibration by bracketing ten unknowns with three analyses of the reference zircon. Reference zircon 91500 (Wiedenbeck et al., 1995) was analysed as an unknown. Both reference zircons were measured with a spot size of 35 μm. The same spot size was used for most of the samples. The spots were pre-ablated prior to each analysis to remove any surface contamination. The masses 202 (to determine ^{204}Hg interference with ^{204}Pb), 204, 206, 207 and 208 were measured. The common ^{204}Pb fraction of total ^{206}Pb was generally below 1%. A recognized ^{238}U/^{235}U ratio is 137.88 (Cowan and Adler, 1976) to estimate ^{235}U. The data reduction was done offline using an in-house spreadsheet file to correct for elemental fractionation, instrumental mass bias and drift.

The measured ^{206}Pb/^{238}U (0.183 ± 0.004; n = 26) and ^{207}Pb/^{206}Pb (0.0754 ± 0.0015) of the internal reference zircon 91500 (n = 26) match their recommended values (0.1792 ± 2 and 0.07488 ± 2 respectively; Wiedenbeck et al., 1995). Concordia diagrams were constructed using ISOPLOT 4.15 (Ludwig, 2003). All U—Pb age data is presented in Table A3 (Appendix A).

3.3. Bulk rock Rb—Sr isotopes

Around 90 mg of finely powdered whole rock powder of each sample were digested in 40% HF inside Parr® bombs after adding ^{87}Rb—^{84}Sr whole rock spike solution. Parr bombs were kept in an oven at 200 °C for two days. Afterwards, these samples underwent a digestion procedure using concentrated HF, HNO_3 and HCl solutions separately for two days each at 100 °C. Each step was carried out after drying the samples on a hotplate at 100 °C. After drying the samples, they were loaded on DOWEX® AG 50 W-X8 (200–400 mesh) cation columns to separate Rb and Sr. The loading reagent was 2.5 M HCl. Rubidium and Sr cuts were collected using 2.5 M HCl with a distinct eluting step in between.

Strontium isotopes were measured in static mode on a Thermo Scientific Triton Plus® Thermal Ionization Mass Spectrometer (TIMS) at the Institute of Geological Sciences, University of Bern, Switzerland. Strontium cuts were loaded on zone-refined Re single filaments using 6.4 M HCl with Ta-oxide as an activator. The Sr isotope ratios were corrected for mass bias using exponential law and iteration (Stracke et al., 2014). The NIST standard SRM® 987 yielded ^{87}Sr/^{86}Sr = 0.710326 ± 0.000010 (2SD; n = 24) which was corrected for the offset with a recommended value of 0.710245. The same offset was also calculated for the rock standards (BCR-2; ^{87}Sr/^{86}Sr = 0.704987 ± 0.000011; Raczek et al., 2003) and the samples. Rubidium concentrations were measured on a Thermo Scientific® Neptune Plus® Multi Collector Inductively Coupled Plasma Mass Spectrometer (MC ICPMS) present at the Institute of Geological Sciences, University of Bern, Switzerland. The total procedural blanks were < 200 pg for Rb and Sr and thus negligible for the analysed samples. The isotope ratios were corrected for mass bias by the standard-sample-standard bracketing method using the exponential law.

3.4. Bulk rock Lu—Hf isotope measurements

The Lu—Hf isotope whole rock measurements were carried out at the Institute of Geological Sciences, University of Bern, Switzerland. Around 100 mg of each finely powdered sample was spiked with ^{176}Lu—^{180}Hf and ^{149}Sm—^{150}Nd spikes in Savillex® beakers by keeping an empiric error magnification of ~1.5–2 (Stracke et al., 2014). These samples underwent an initial digestion procedure for two days in concentrated HF at 200 °C inside Parr® bombs. After drying these samples on a hotplate, they went through dissolution procedures with concentrated HF, HNO_3 and HCl acids (each separately for ~2 days) at 120 °C. After dissolution, the samples were subjected to Lu—Hf column chemistry using 1 M HCl + 0.1 M HF as the loading reagent. The resin DOWEX® AG 50 W-X8 (200–400 mesh) was used to separate HFSE (Zr, Hf), LREE (Sm—Nd) and HREE (Lu), modified according to the procedure in Bast et al. (2015).

Hafnium and Lu isotope compositions were measured on Thermo Scientific® Neptune Plus® Multi Collector ICPMS at the Institute of Geological Sciences, University of Bern, Switzerland. Dry plasma mode using a Cetac Aridus II desolvation system was used for efficient sample introduction and sensitivity during the measurements on the multi collector ICPMS. Background measurements of the washing acid reagents, 0.56 M HNO_3 + 0.3 M HF (for Hf) and 0.5 M HNO_3 (for other isotopes), were subtracted from each measurement of sample and standard solutions. A long-term analytical session of JMC 475 over a year gave averages of ^{176}Hf/^{177}Hf = 0.282147 ± 0.000006 (2SD; n = 24) which is within the range of agreed values (e.g., 0.282163 ± 0.000026; Chu et al. (2002)). The Hf isotope ratios were corrected for mass bias using exponential law with a normalization ratio of ^{179}Hf/^{177}Hf = 0.7325 (Patchett and Tatsumoto, 1981). The JMC standard for Lu were mixed with Yb standard (JMC) and diluted according to the Yb/Lu ratios of the samples. The total procedural blanks were < 80 pg for Lu and and < 150 pg for Hf, which were used for blank correction on the samples. The international rock reference standard BCR-2 gave an average ^{176}Hf/^{177}Hf = 0.282850 ± 0.000004 (2SD; spiked) and ^{176}Hf/^{177}Hf = 0.282865 ± 0.000005 (2SD; unspiked), which is in agreeable range (0.282859 ± 0.000009; Chu et al. (2002)). The ε_{Hf} were calculated based on the rock's U—Pb concordant zircon age and constraints such as (^{176}Lu/^{177}Hf)$_{CHUR}$ = 0.0336 and (^{176}Hf/^{177}Hf)$_{CHUR}$ = 0.282785 (Bouvier et al., 2008) and a ^{176}Lu decay constant of 1.867 × 10^{-11} a^{-1}(Scherer et al., 2001).

3.5. Lead isotope measurements

For common Pb isotope measurements, feldspar grains (K-feldspar and plagioclase of ~15–20 mg each) of each sample were hand-picked from a fraction that was already separated by magnetic separation. The feldspar grains were carefully evaluated under a binocular microscope and the cleanest material was selected for analysis. The grains were cleaned with ethanol followed by leaching steps to remove radiogenic Pb that can be added by mica and secondary clays formed due to weathering (modified from Villa and Hanchar (2013)). Before leaching, the grains of each sample were kept in 2 ml aquaregia (1 ml 6 M HCl + 1 ml 7 M HNO_3) solution at 100 °C for ~12 hours on the hotplate. Afterwards, the grains were leached with a mixture of ~10 drops of Milli-Q, ~2 drops of concentrated HNO_3 and 2–3 drops of concentrated HF after keeping the solution (with the grains) on the hotplate at 100 °C for 10 minutes. The last leaching step was with ~5–6 drops of Milli-Q, 1 drop of HNO3 and 15 drops of concentrated HF. The solution was kept on the hotplate for ~2 minutes until 20–30% of the

grains were dissolved. Afterwards, the grains were completely dissolved in concentrated HF for 24 hours and dried. The samples were loaded on columns packed with DOWEX® 1-X8 anion resin with a few drops of 3 M HCl as the loading reagent. Solutions of 1 M HBr and subsequently 3 M HCl were used for wash-in before collecting Pb in 6 M HCl.

Lead isotopes were measured on a Neptune Plus® Multi Collector ICPMS at the Institute of Geological Sciences, University of Bern. The Pb standard (NIST SRM® 981) was doped with Tl standard in the ratio of 10:1 to measure along with the samples for efficient correction for mass fractionation. Mass bias correction was done with the measured $^{205}Tl/^{203}Tl$ (e.g., Rehkämper and Mezger, 2000). Interference of ^{204}Hg was corrected online after measuring ^{202}Hg. Analytical on-peak-zero measurements were subtracted from standard and sample measurements to correct for excess Pb in the reagent solution. All acids were prepared from low-blank reservoirs of Milli-Q, HNO_3 and HCl (0.08 pg, 0.5 pg and 0.5 pg respectively on ^{208}Pb). The procedural blank on ^{208}Pb was ~20 pg. Measurements of Pb ratios of NIST SRM® 981 yielded $^{207}Pb/^{206}Pb = 0.91482 \pm 0.00009$ (2SD, $n = 19$; Pandey et al., 2019), using a fractionation correction based on $^{205}Tl/^{203}Tl = 2.387$.

3.6. Single grain Hf isotope analysis of zircon

Two different processing and analytical techniques were used for the measurements of Hf isotopes in zircon. One method involved in-situ measurements of mounted zircon grains using a Thermo Scientific® Neptune Plus® Multi Collector Inductively Coupled Plasma Mass Spectrometer (MC ICPMS) coupled with an ESI 193 nm excimer laser ablation source at the Indian Institute of Technology, Kharagpur, India. For in-situ analyses, the spots were chosen next to the spots analysed for U—Pb ages (Fig.B2; Appendix B) to sample the same chemical/age zone for both U—Pb and Hf isotope measurements to choose robust concordant ages for calculating initial Hf ratios (e.g., Vervoort and Kemp, 2016). The analyses were performed in time-resolved mode with each measurement consisting of measurement of gas background for 25 s with the laser turned off and a window for sample signal acquisition for 50 s with the laser turned on. With a signal integration time of 0.524 s/cycle, approximately 50 isotope ratios were acquired for the background and ca. 100 ratios for the peak signal domain during analyses. The optimum laser ablation was carried out at 4–5 J/cm^2 beam energy density and 10 Hz repetition rate. Instrumental mass-bias was corrected using the exponential law while instrumental drift was corrected by sample standard external bracketing using the homogenous, well-characterized matrix matched 91,500 reference zircon (Wiedenbeck et al., 1995). The correction for isobaric interference of ^{176}Yb was done using a natural $^{176}Yb/^{173}Yb = 0.786956$ ratio (Thirlwall and Anczkiewicz, 2004). The mass bias factor for Yb (βYb) was calculated from the measured $^{173}Yb/^{171}Yb$ ratio and a reference value $^{173}Yb/^{171}Yb = 1.123456$ (Thirlwall and Anczkiewicz, 2004). The mass bias factor for Hf (βHf) was calculated based on the exponential law and normalizing ratio $^{179}Hf/^{177}Hf = 0.7325$ (Patchett and Tatsumoto, 1981). Interference of ^{176}Lu on ^{176}Hf was corrected using the interference-free ^{175}Lu and the natural $^{176}Lu/^{175}Lu = 0.02656$ (Chu et al., 2002). The Plešovice and Temora-2 reference zircons measured as unknown, gave average $^{176}Hf/^{177}Hf$ of 0.282481 ± 0.000027 and 0.282681 ± 0.000043 respectively (Table A4; Appendix A) that are within uncertainty of the recommended values (Fisher et al., 2014).

Robustness of the interference correction for Yb was tested by doping JMC 475 Hf isotope standard with varying amounts of Yb ($^{176}Yb/^{177}Hf$ ratios up to 0.34). The mean $^{176}Hf/^{177}Hf$ of the Yb-doped JMC-475 solutions was identical to the un-doped JMC 475 measurements and individual analyses did not show any correlation between $^{176}Hf/^{177}Hf$ and $^{176}Yb/^{177}Hf$ (Table A4; Appendix A). The Hf isotope composition of reference zircons Temora-2 and Plešovice were analysed as unknowns. The $^{176}Yb/^{177}Hf$ ratios of these two reference zircons range from zero to nearly 0.1, which agrees with the range of $^{176}Yb/^{177}Hf$ ratios of sample zircons (Table A4; Appendix A). No correlation was observed between the interference monitors and $^{176}Hf/^{177}Hf$ of reference as well as sample zircons. There was no observed correlation between $^{176}Hf/^{177}Hf$ and $^{178}Hf/^{177}Hf$ (Table A4; Appendix A), which indicates that mass bias was adequately corrected for.

For the second method, selected zircon grains were analysed conventionally by MC-ICPMS at the University of Bern, Switzerland after dissolution and separation of Lu and Hf by ion-exchange chromatography. Zircon grains were selected from samples that showed no optically detectable evidence of inheritance and their U—Pb systematics yielded concordant ages or the analyses fall on a well-defined discordia line. One to two concordant grains were selected from some of the granitoid samples after in-situ U—Pb dating. These grains were separated from the mount, cleaned with ethanol and digested in 40% HF after transferring them to micro-capsules. These micro-capsules were kept in Parr bombs at 200 °C for two days. A $^{176}Lu—^{180}Hf$ tracer was added prior to digestion. After drying, concentrated HNO_3 and HCl were added in two separate steps with drying steps in between. After dissolution, the samples were subjected to ion exchange chromatography to obtain a clean Hf separate. Lutetium and Hf isotope compositions were measured on Neptune Plus Multi Collector ICPMS. An average of $^{176}Hf/^{177}Hf = 0.282185 \pm 0.000006$ (2SD; $n = 8$) was obtained for JMC 475, which is within the range of agreed values (0.282163 ± 0.000026; Chu et al., 2002). Total procedural blanks were < 150 pg.

4. Results

4.1. Major and trace elements

The major and trace element abundances for all samples are presented in Table 1. Based on their normative mineralogy, the granitoids in the western Dharwar Craton include granites and trondhjemites with minor tonalites (Fig.B3; Appendix B). There is a clear separation of granitoids into two groups based on their Al_2O_3 contents (Fig. 2a) which has also been observed in previous studies (Jayananda et al., 2015; Jayananda et al., 2018). Most of the granitoids have Al_2O_3 concentrations from 13.33 to 16.09 wt%. However, some trondhjemites have significantly lower Al_2O_3 concentrations from 10.72 to 11.35% (Table 1). These low-Al trondhjemites have high SiO_2 contents (75.91–78.04 wt%). The SiO_2 concentrations of the other, high-Al granitoids are significantly lower: trondhjemites range from 69.89 to 72.77 wt%, granites from 70.09 to 75.52 wt% and tonalites from 63.88 to 70.87 wt%. Tonalites have lower Na_2O, K_2O and higher MgO, FeO and CaO contents compared to the trondhjemites and granitic gneisses in the craton (Fig. 2b, c, d, e, & f). The major element abundances of silicic volcanic rocks are similar to those of the intrusive granitoids in the craton. The granitoid suite shows a typical differentiation trend of decreasing MgO, FeO and CaO with increasing SiO_2 is observed (Fig. 2d, e & f). There is no well-developed trend observed for Na_2O contents in rocks with increasing SiO_2 content (Fig. 2b). Some granitic rocks with significantly high K_2O contents have low Na_2O contents (GHH 22.1, GHH 22.3, SG 43.1; Fig. 2b & c).

Most granitoid rocks from the craton show LREE enrichment and HREE depletion (Fig. 3a & c). Some tonalites have no Eu anomaly (Eu/Eu* = 1.0–1.1) and the felsic volcanic rocks have no or slightly positive Eu/Eu* (Table 1; Fig. 3b & d). Most of the granites in the craton show a significant negative Eu anomaly ((Eu/Eu* = 0.4–0.9). Trondhjemites and tonalites have high Sr/Y (4.3–90.0), high La/Yb (4.5–100.0) and low Nb and Ta contents (Table 1; Fig. 4). The major and trace element abundances and their variations among the evolved magmatic rocks are typical for granitoids that formed by partial melting of a basaltic source rock by magmatic differentiation (Figs. 2,3; Ravindran et al., 2021; McDonough and Sun, 1995; Sun and McDonough, 1989).

A distinct group among these intrusive and extrusive granitoids are low-Al trondhjemites. In addition to their distinctly low Al_2O_3 contents, they have distinctly less fractionated REEs compares to all other granitoids (Fig. 3b & d). They also have significantly low Sr/Y (0.6–2.1) and

Table 1
Major (wt%), minor and trace (ppm) element compositions of granitoid and felsic volcanic rocks in the western Dharwar Craton.

	Det. limit	SG 32.1	SG 32.2	SG 34.1	CHK 36.1	CHK 38.1	SG 43.1	HNL 6.1	HNL 6.3	HNL 7.1	HNL 7.2
SiO_2	0.01 (wt%)	72.49	70.78	69.32	70.09	75.91	75.34	63.88	72.21	69.89	74.00
Al_2O_3	0.01 (wt%)	14.71	15.64	15.24	15.29	10.93	13.33	14.33	14.95	16.09	14.46
Fe_2O_3(T)	0.01 (wt%)	2.41	2.78	4.19	3.02	4.22	1.64	6.00	1.94	2.61	0.88
MnO	0.001 (wt%)	0.03	0.03	0.06	0.03	0.05	0.03	0.08	0.02	0.04	0.02
MgO	0.01 (wt%)	0.62	0.81	0.99	1.20	1.00	0.29	5.02	1.00	0.90	0.12
CaO	0.01 (wt%)	2.06	2.57	3.33	1.73	2.00	1.20	3.25	1.96	1.98	1.23
Na_2O	0.01 (wt%)	4.32	4.97	4.74	4.74	3.54	3.47	3.34	5.00	4.54	4.13
K_2O	0.01 (wt%)	3.08	1.64	1.54	2.61	1.30	4.61	1.04	1.25	2.02	4.48
TiO_2	0.001 (wt%)	0.34	0.43	0.44	0.39	0.84	0.23	0.46	0.21	0.39	0.07
P_2O_5	0.01 (wt%)	0.08	0.11	0.14	0.14	0.24	0.06	0.07	0.22	0.13	0.02
LOI		0.58	0.59	0.68	1.04	0.51	0.33	2.61	0.97	1.15	0.43
Total		100.7	100.3	100.7	100.3	100.5	100.5	100.1	99.7	99.8	99.8
Rb	1 (ppm)	60	50	65	61	35	183	41	43	132	139
Sr	2 (ppm)	411	438	302	346	227	140	255	306	268	175
Y	0.5 (ppm)	10.4	11.3	25.2	14.3	111.0	32.9	14.7	10.1	8.2	7.1
Zr	1 (ppm)	182	206	231	207	464	158	118	260	211	62
Nb	0.2 (ppm)	7.7	8.1	12.7	7.1	23.3	13.0	6.5	1.9	4.4	2.9
Cs	0.1 (ppm)	0.4	0.5	2.3	0.8	0.8	5.2	0.4	0.4	4.2	1.2
Ba	2 (ppm)	540	256	120	511	115	644	113	147	149	198
La	0.05 (ppm)	50.2	62.1	63.7	41.7	50.2	72.0	21.5	72.1	35.1	9.9
Ce	0.05 (ppm)	84.7	105.0	107.0	74.7	107.0	131.0	39.9	136.0	60.3	18.8
Pr	0.01 (ppm)	8.8	11.1	11.1	8.0	14.4	14.0	4.2	13.9	6.1	2.1
Nd	0.05 (ppm)	29.3	36.0	36.3	28.2	59.8	44.5	15.3	44.6	20.2	7.8
Sm	0.01 (ppm)	4.74	5.91	6.16	5.22	15.10	7.50	3.27	7.18	3.39	1.89
Eu	0.005 (ppm)	1.11	1.19	1.29	1.17	2.51	1.08	1.02	1.32	0.84	0.57
Gd	0.01 (ppm)	3.56	4.11	5.31	4.11	17.40	6.41	2.93	4.56	2.27	1.67
Tb	0.01 (ppm)	0.45	0.53	0.83	0.59	3.04	1.04	0.46	0.51	0.28	0.22
Dy	0.01 (ppm)	2.31	2.53	4.82	3.19	20.20	6.19	2.76	2.38	1.47	1.21
Ho	0.01 (ppm)	0.40	0.43	0.93	0.56	4.46	1.23	0.53	0.37	0.25	0.24
Er	0.01 (ppm)	1.00	1.04	2.55	1.44	13.50	3.46	1.60	0.95	0.75	0.63
Tm	0.005 (ppm)	0.13	0.13	0.37	0.19	2.02	0.51	0.23	0.12	0.11	0.09
Yb	0.01 (ppm)	0.74	0.73	2.42	1.20	13.20	3.36	1.60	0.76	0.67	0.60
Lu	0.002 (ppm)	0.09	0.10	0.38	0.16	2.00	0.52	0.24	0.13	0.10	0.10
Hf	0.1 (ppm)	4.70	5.10	5.60	5.30	13.00	4.90	3.20	7.00	4.40	2.20
Ta	0.01 (ppm)	0.34	0.26	1.36	0.79	1.61	1.06	0.62	0.07	0.35	0.14
Pb	5 (ppm)	15	13	13	8	10	40	6	9	8	17
Th	0.05 (ppm)	15.00	19.40	14.90	8.64	7.95	22.30	7.58	23.30	10.30	4.47
U	0.01 (ppm)	0.97	1.19	2.72	0.78	2.15	5.53	1.07	1.14	1.29	0.71
Nb/Ta		22.65	31.15	9.34	8.99	14.47	12.26	10.48	27.14	12.57	20.71
Sr/Y		39.52	38.76	11.98	24.20	2.05	4.26	17.35	30.30	32.68	24.65
La/Yb		67.84	85.07	26.32	34.75	3.80	21.43	13.44	94.87	52.39	16.52
Zr/Sm		38.40	34.86	37.50	39.66	30.73	21.07	36.09	36.21	62.24	32.80
Eu/Eu*		0.82	0.74	0.69	0.77	0.47	0.47	1.00	0.70	0.92	0.98

	Det. limit	GHH 22.1	GHH 22.3	GHH 22.4	BB 8.1	BB 8.2	SG 26.1	SG 27.1	SG 29.1	SG 30.2	SG 30.3	SG 31.1
SiO_2	0.01 (wt%)	73.10	73.32	7087	69.78	74.07	80.79	74.42	72.77	78.04	76.54	75.52
Al_2O_3	0.01 (wt%)	13.41	13.28	15.03	14.84	13.79	10.89	14.39	14.61	10.72	11.35	14.40
Fe_2O_3 (T)	0.01 (wt%)	2.22	2.15	3.52	2.81	1.60	1.31	1.33	2.16	3.12	3.62	0.80
MnO	0.001 (wt%)	0.04	0.04	0.05	0.03	0.02	0.01	0.02	0.02	0.07	0.08	0.02
MgO	0.01 (wt%)	0.50	0.49	0.88	2.29	1.24	0.06	0.33	0.54	0.54	0.72	0.13
CaO	0.01 (wt%)	1.46	1.49	3.31	1.15	0.91	0.59	1.76	2.62	1.58	1.43	1.36
Na_2O	0.01 (wt%)	3.16	3.13	4.38	4.21	5.10	4.14	4.58	4.76	4.18	4.19	4.99
K_2O	0.01 (wt%)	4.77	4.77	1.35	1.85	1.24	2.38	2.78	1.54	0.94	1.18	3.03
TiO_2	0.001 (wt%)	0.28	0.28	0.38	0.32	0.17	0.11	0.20	0.38	0.62	0.66	0.07
P_2O_5	0.01 (wt%)	0.08	0.08	0.12	0.13	0.06	<0.01	0.07	0.13	0.06	0.07	0.02
LOI		0.53	0.55	0.73	2.34	1.51	0.37	0.61	0.60	0.29	0.49	0.34
Total		99.5	99.6	100.6	99.7	99.7	100.6	100.5	100.1	100.2	100.3	100.7
Rb	1 (ppm)	192	189	90	66	46	37	92	35	25	35	105
Sr	2 (ppm)	166	156	369	24	177	198	314	495	75	83	467
Y	0.5 (ppm)	19.8	20.8	7.4	8.2	11.8	186.0	10.0	5.5	117.0	133.0	12.5
Zr	1 (ppm)	214	213	194	129	95	214	106	150	480	535	59
Nb	0.2 (ppm)	9.8	9.5	4.5	4.1	6.6	23.5	4.5	3.4	18.4	19.8	7.4
Cs	0.1 (ppm)	9.6	8.0	7.6	1.0	0.7	0.2	3.8	0.8	1.2	1.6	2.0
Ba	2 (ppm)	530	511	129	174	90	619	392	282	95	160	764
La	0.05 (ppm)	65.8	66.3	34.5	17.2	16.8	57.2	25.8	28.0	38.7	44.0	6.2
Ce	0.05 (ppm)	121.0	122.0	60.1	34.9	29.5	128.0	45.8	52.8	87.1	95.5	11.9
Pr	0.01 (ppm)	13.1	13.1	6.2	3.4	3.3	17.8	5.1	6.2	11.7	13.0	1.5
Nd	0.05 (ppm)	42.7	43.4	21.3	12.2	11.5	75.4	18.5	23.0	51.5	55.4	6.1
Sm	0.01 (ppm)	6.86	7.11	3.49	2.31	2.39	21.70	3.56	4.32	14.30	15.50	1.65
Eu	0.005 (ppm)	0.89	0.86	1.05	0.86	0.67	2.86	0.95	1.13	3.54	3.90	0.47
Gd	0.01 (ppm)	5.09	5.33	2.46	1.87	2.03	28.60	2.86	3.11	17.30	18.80	1.78
Tb	0.01 (ppm)	0.72	0.73	0.31	0.26	0.32	5.44	0.40	0.35	3.15	3.48	0.31
Dy	0.01 (ppm)	4.12	4.10	1.52	1.47	1.98	36.00	2.15	1.54	21.40	23.60	2.16
Ho	0.01 (ppm)	0.81	0.77	0.28	0.28	0.40	7.62	0.38	0.20	4.64	5.09	0.44

(*continued on next page*)

Table 1 (*continued*)

	Det. limit	GHH 22.1	GHH 22.3	GHH 22.4	BB 8.1	BB 8.2	SG 26.1	SG 27.1	SG 29.1	SG 30.2	SG 30.3	SG 31.1
Er	0.01 (ppm)	2.23	2.27	0.79	0.81	1.13	21.70	1.01	0.44	13.90	15.20	1.28
Tm	0.005 (ppm)	0.33	0.33	0.11	0.12	0.17	2.98	0.15	0.05	2.10	2.27	0.20
Yb	0.01 (ppm)	2.15	2.38	0.64	0.82	1.17	19.50	0.94	0.28	14.30	15.40	1.38
Lu	0.002 (ppm)	0.31	0.35	0.09	0.12	0.17	3.01	0.14	0.04	2.23	2.39	0.21
Hf	0.1 (ppm)	6.30	6.20	4.60	2.90	2.70	8.60	3.20	3.70	11.70	13.50	2.10
Ta	0.01 (ppm)	1.65	1.43	0.42	0.45	0.86	1.95	0.63	0.23	1.62	1.82	0.61
Pb	5 (ppm)	19	20	8	<5	<5	7	18	8	7	8	39
Th	0.05 (ppm)	17.10	17.20	5.21	4.08	5.48	11.50	7.52	5.65	7.36	8.19	2.84
U	0.01 (ppm)	2.15	2.04	0.64	0.55	1.09	2.02	3.12	0.53	1.92	1.78	3.02
Nb/Ta		5.94	6.64	10.71	9.11	7.67	12.05	7.14	14.78	11.36	10.88	12.13
Sr/Y		8.38	7.50	49.86	21.59	16.78	0.13	31.40	90.00	0.64	0.62	37.36
La/Yb		30.60	29.08	53.91	20.98	14.36	2.93	27.45	100.00	2.71	2.86	4.49
Zr/Sm		31.20	29.96	55.59	55.84	39.75	9.86	29.78	34.72	33.57	34.52	35.76
Eu/Eu*		0.46	0.42	1.09	1.27	0.93	0.35	0.91	0.94	0.69	0.70	0.84

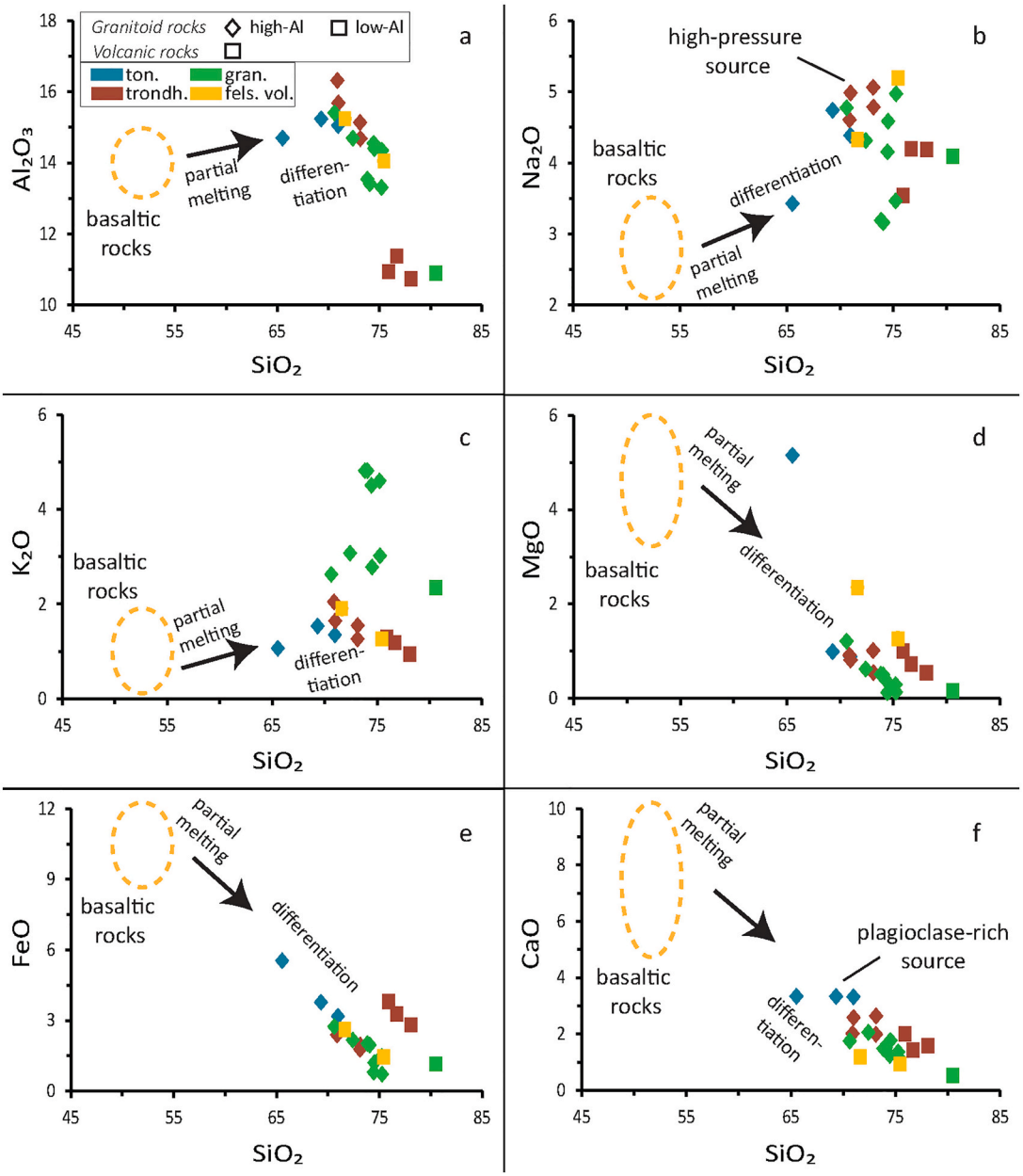

Fig. 2. Major element variation diagrams of granitoid and felsic volcanic rocks based on whole rock major element compositions given in Table 1. All oxides are presented in wt%, after excluding loss on ignition (LOI). Yellow dashed circle represents the major element signatures of basaltic rocks in the western Dharwar Craton (Ravindran et al., 2021). (For interpretation of the references to colour in this figure legend, the reader is referred to the web version of this article.)

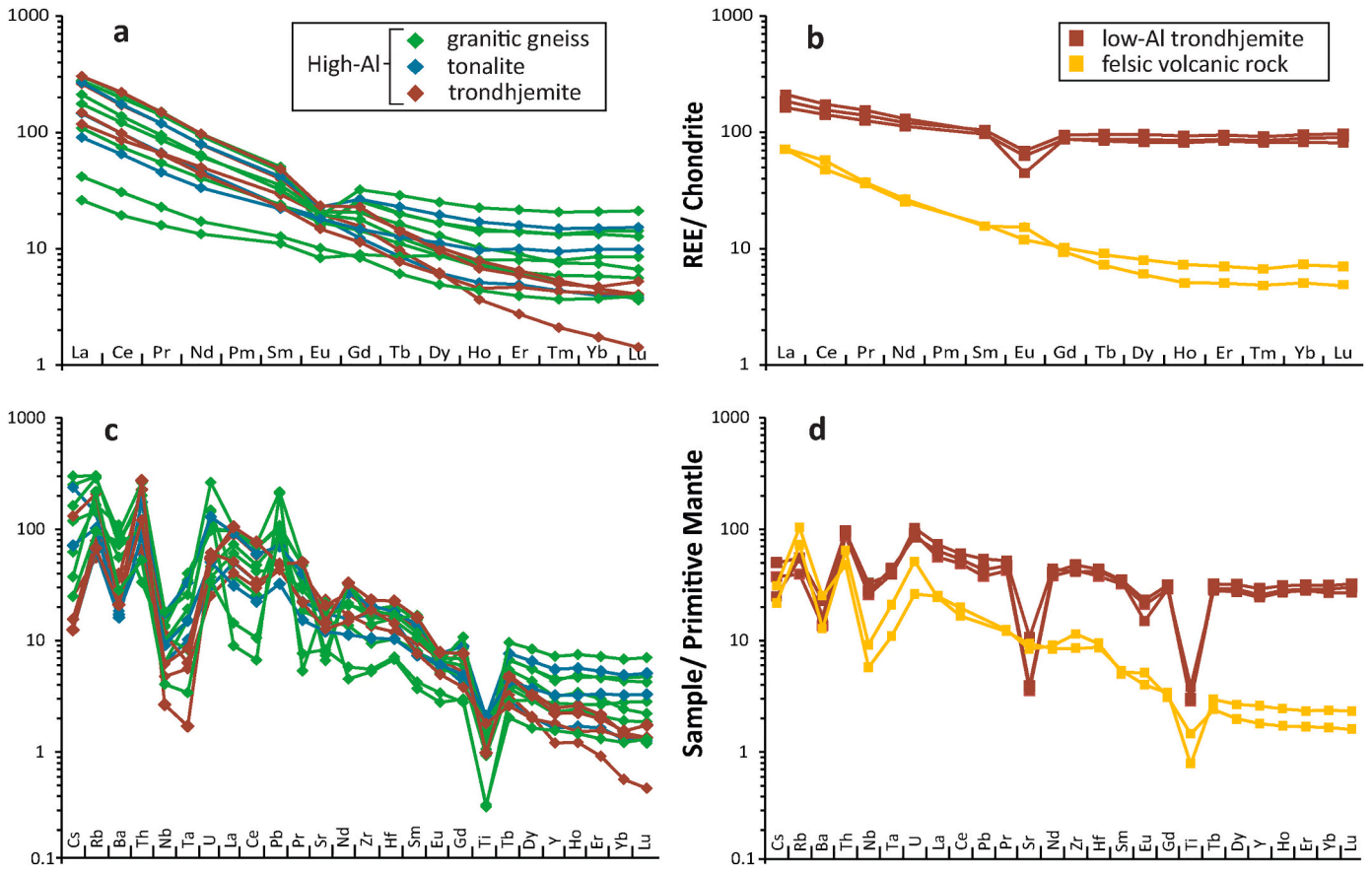

Fig. 3. (a, b) chondrite normalized REE (c, d) primitive mantle normalized multi-element plots of granitoid and felsic volcanic rocks in the western Dharwar Craton.

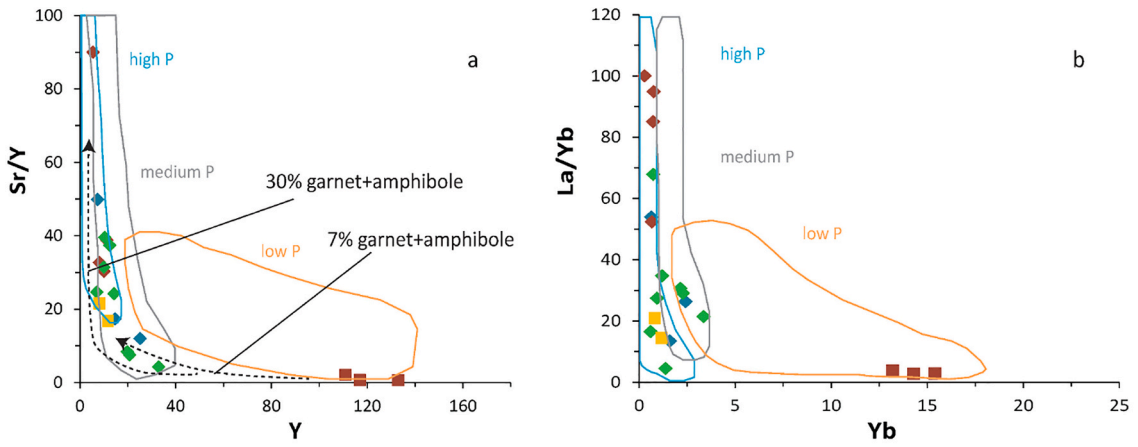

Fig. 4. (a) Sr/Y vs. Y and (b) La/Yb vs. Yb diagrams showing different pressure fields for partial melting (after Moyen, 2011). Symbols of the samples are the same as in 3. The diagrams illustrate pressure ranges for partial melting of mafic precursor(s) of the granitoids of the western Dharwar Craton.

La/Yb (2.7–2.8) ratios along with relatively high Nb and Ta contents (Table 1; Fig. 4). The combined major and trace element characteristics indicate a petrogenetic path for the low-Al trondhjemites that is distinctly different from the other granitoids.

4.2. Zircon U—Pb ages

4.2.1. Granitoids (TTGs and other gneisses)

Uranium-Pb age and isotope data from magmatic zircons in 21 rock samples are given in Table A3 (Appendix A). Zircon grains with magmatic zoning from two well-preserved tonalite samples from the Ghattihosahalli and Holenarsipur regions of the western Dharwar Craton yielded concordant U—Pb ages of 3197 ± 11 Ma (Fig. 5a) and 3385 ± 13 Ma (Fig. 5b), respectively. Both samples have lower intercepts with Concordia at ~515 Ma. Zircons from granitic rocks in the Ghattihosahalli area yielded concordant ages of 3010 ± 25 Ma (lower intercept at 1056 ± 530 Ma) and 3026 ± 26 Ma (poorly defined lower intercept at 765 ± 2800 Ma) (Table A3; Appendix A). Two different trondhjemite bodies from the Holenarsipur-Gorur area yielded similar U—Pb ages of 3178 ± 10 Ma and 3163 ± 18 Ma (Fig.B4a &b; Appendix B). Granites from the Gorur area are older and have concordant zircon ages of 3321 ± 16 Ma and 3362 ± 42 Ma. The felsic volcanic rocks yield

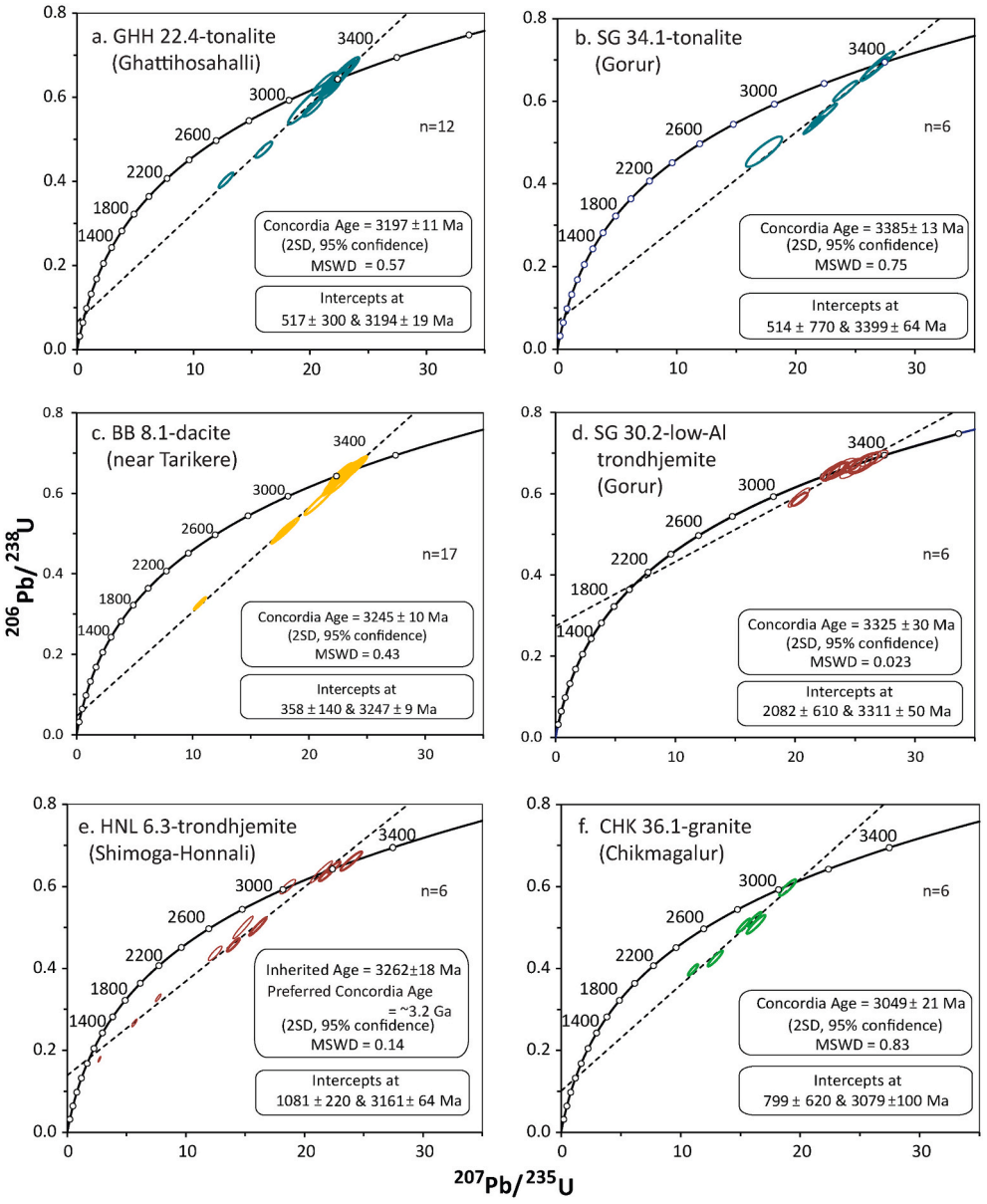

Fig. 5. Concordia diagrams showing U—Pb ages of magmatic zircons in granitoids and felsic volcanic rocks from the western Dharwar Craton. Only the highlighted symbols are considered for calculating concordant ages. 'n' refers to the number of analyses used for constructing the Discordia line.

concordant U—Pb zircon ages of 3245 ± 10 Ma and 3244 ± 9 Ma (Fig. 5c & B4c (Appendix B)) that define the time of deposition of the Sargur Group. These rocks have lower intercept ages of 358 (±140) Ma and 206 (±310) Ma respectively. The low-Al trondhjemites from the Holenarsipur area yielded distinctly older ages of ~3.33 Ga (3 samples; Table A3, Appendix A) with the oldest sample having a Concordia age of 3325 ± 30 Ma (Fig. 5d). Their lower intercept ages range from Paleo- to Mesoproterozoic. Most zircon grains from a trondhjemite from the Shimoga region (Honnali dome) define a discordia with an upper intercept age of 3262 ± 18 Ga (Fig. 5e), but some grains are even slightly older. CL images of these older grains indicated that they are inherited. A granitic gneiss from the Chikmagalur area is younger (3049 ± 21 Ma; Fig. 5f) than the other granitic gneisses in the craton (Table A3; Appendix A). The granitic gneiss from the Shravanabelagola dome has a Concordia age of 3107 ± 20 Ma with the discordia line not tightly constrained (Fig.B4d). Most of the TTGs from the Gorur-Holenarsipur area define lower intercept ages in the Paleozoic (Fig. 5 b & d) whereas the granites have Proterozoic lower intercept ages (Fig. 5f). The zircon suites of low-Al trondhjemites also have lower intercept ages in the Proterozoic.

4.2.2. *Sedimentary rocks*

Oscillatory and sector zoning as indicators of primary growth zoning, U concentrations and identical $^{207}Pb/^{206}Pb$ ages of different detrital zircon grains in each sediment sample were considered to identify the least disturbed grains (Nemchin et al., 2006). Using these selection criteria, a total of 144 detrital zircon grains from six sedimentary rocks were analysed to determine their U—Pb ages. The analytical information for zircons from meta-sedimentary rocks from the greenstone belts is given in Table A3 (Appendix A). The maximum $^{207}Pb/^{206}Pb$ ages obtained are 3498 ± 42 Ma and 3485 ± 41 Ma for zircon grains from a meta-sedimentary rock (Fig. 6a) from the Holenarsipur schist belt. Detrital zircon grains from conglomerates in the Holenarsipur and Ghattihosahalli schist belts yield similarly old $^{207}Pb/^{206}Pb$ ages of 3451 ± 16 Ma and 3467 ± 18 Ma (Fig. 6b & c). Zircons from a fuchsite quartzite and a quartzite yielded the oldest ages (Fig. 6d & f) reported

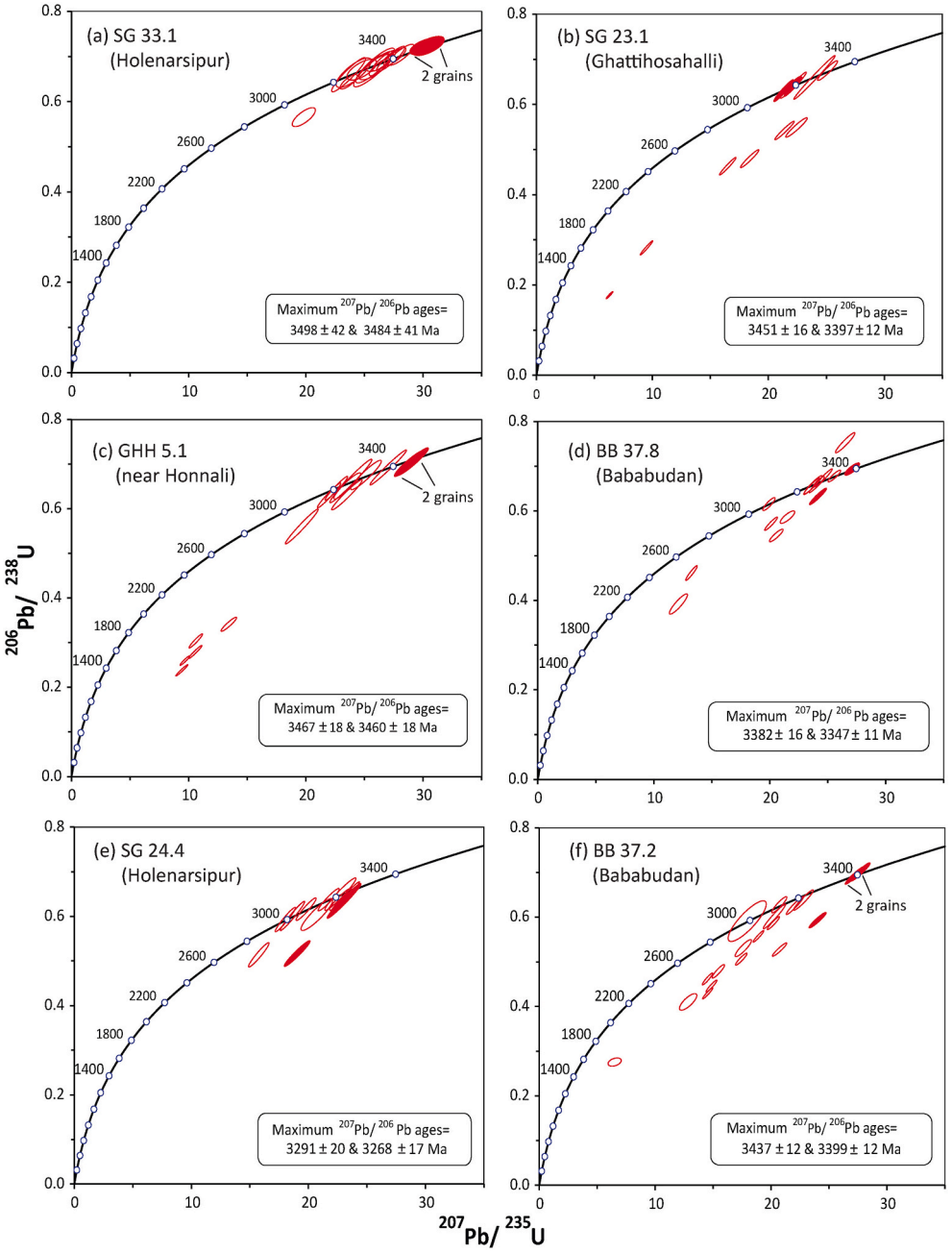

Fig. 6. Concordia diagrams showing U—Pb ages of detrital zircons in sedimentary rocks belonging to the Sargur and Bababudan Groups in the western Dharwar Craton. Filled symbols indicate the grains with the oldest $^{207}Pb/^{206}Pb$ ages.

from the Bababudan schist belt which are 3382 ± 16 Ma and 3437 ± 12 Ma. In some samples, zircon grains show disturbance of the U—Pb isotope system as a result of Pb-loss and define discordia lines with Proterozoic lower intercept ages (Fig. 6f). A quartzite from the Holenarsipur schist belt gave $^{207}Pb/^{206}Pb$ ages (Fig. 6e) similar to the formation age of the Sargur Group (~3.25 Ga; Fig. 5c). All these ages combined indicate that the major episode of felsic crust formation in the region occurred between 3.40 and 3.15 Ga with some minor evolved granites forming at ca. 3.05 Ga.

4.3. Bulk rock Lu—Hf isotope systematics

Whole rock Lu—Hf isotope compositions of rocks older than 3.25 Ga have radiogenic initial Hf isotopes (ε_{Hf} = +1.8 ± 0.6 to +5.8 ± 0.4), indicating a mildly to significantly depleted source. Rocks younger than 3.25 Ga have a slightly lower range of εHf_i (−0.6 ± 0.1 to +7.8 ± 0.3) (Table 2, Fig. 7), indicating an origin from a mildly enriched source. Whole rock Lu—Hf isotope compositions of granitoids from the craton have not been published so far and these εHf_i values and initial ε_{Nd} values reported so far (e.g., Dey, 2013; Jayananda et al., 2015) fit in the terrestrial magmatic space (Vervoort et al., 2011).

4.4. Hafnium isotope constraints from magmatic zircon

Mean initial ε_{Hf} values of zircon measured in-situ for the granitoid samples (Fig. 8a) range from εHf_i = −0.4 ± 0.7 to +8.6 ± 0.9 for crystallization ages from 3.4 Ga to 3.0 Ga. Whole rock εHf_i values of each individual sample are compared with their zircon εHf_i values obtained by in-situ laser technique and/or bulk grain dissolution technique. Most of the samples have their whole rock and bulk zircon εHf_i values fitting

Table 2
Whole rock Lu—Hf isotope compositions of granitoids and felsic volcanic rocks in the western Dharwar Craton.

Sample	Age (Ma)	Lu/Hf	$^{176}Lu/^{177}Hf$	±2 SD	$^{176}Hf/^{177}Hf$	±2 SD	$(^{176}Hf/^{177}Hf)_i$	εHf_i	±2 SD
GHH 22.1	3026(±26)	0.0513	0.00728	0.00002	0.281271	0.000003	0.280848	+0.6	0.2
GHH 22.3	3010(±25)	0.0484	0.00687	0.00002	0.281253	0.000004	0.280856	+0.5	0.2
GHH 22.4	3197(±11)	0.0203	0.00288	0.00001	0.280983	0.000007	0.280806	+3.1	0.1
SG 27.1	3350(±11)	0.0321	0.00455	0.00002	0.281033	0.000005	0.280739	+4.5	0.2
SG 29.1	3178(±10)	0.0090	0.00127	0.00000	0.280793	0.000004	0.280715	−0.55	0.1
SG 31.1	3302(±25)	0.0758	0.01075	0.00004	0.281496	0.000004	0.280812	+5.8	0.4
SG 32.1	3160(±12)	0.0181	0.00257	0.00001	0.280970	0.000004	0.280814	+2.5	0.1
SG 32.2	3163(±10)	0.0057	0.00181	0.00000	0.280908	0.000004	0.280798	+2.1	0.1
SG 34.1	3385(±13)	0.0592	0.00840	0.00002	0.281143	0.000004	0.280595	+0.1	0.2
SG 43.1	3107(±20)	0.0815	0.01156	0.00003	0.281689	0.000005	0.280998	+7.8	0.3
HNL 6.1	3210	0.0587	0.00833	0.00003	0.281377	0.000003	0.280859	+5.7	0.3
HNL 6.3	3200(±18)	0.0126	0.00179	0.00001	0.280973	0.000003	0.280863	+5.2	0.1
CHK 36.1	3049(±21)	0.0294	0.00417	0.00002	0.281049	0.000005	0.280805	−0.4	0.1
SG 30.2	3325(±30)	0.1582	0.02246	0.00006	0.282123	0.000005	0.280685	+1.8	0.6
SG 30.3	3327(±16)	0.1439	0.02043	0.00006	0.282085	0.000004	0.280776	+5.2	0.5
CHK 38.1	3335(±20)	0.1443	0.02048	0.00006	0.282014	0.000004	0.280698	+2.6	0.5
BB 8.1	3245(±10)	0.0412	0.00584	0.00001	0.281168	0.000005	0.280803	+4.3	0.1
BB 8.2	3244(±9)	0.0479	0.00679	0.00001	0.281233	0.000003	0.280810	+4.6	0.1

Ages correspond to U—Pb concordant zircon ages of the respective rock sample. Age assigned to sample HNL 6.1 is the upper intercept age in the absence of a concordia age. The notation 'i' in $(^{176}Hf/^{177}Hf)_i$ and εHf_i correspond to the time of formation of the rock, which is the U—Pb zircon age of the respective rock sample.

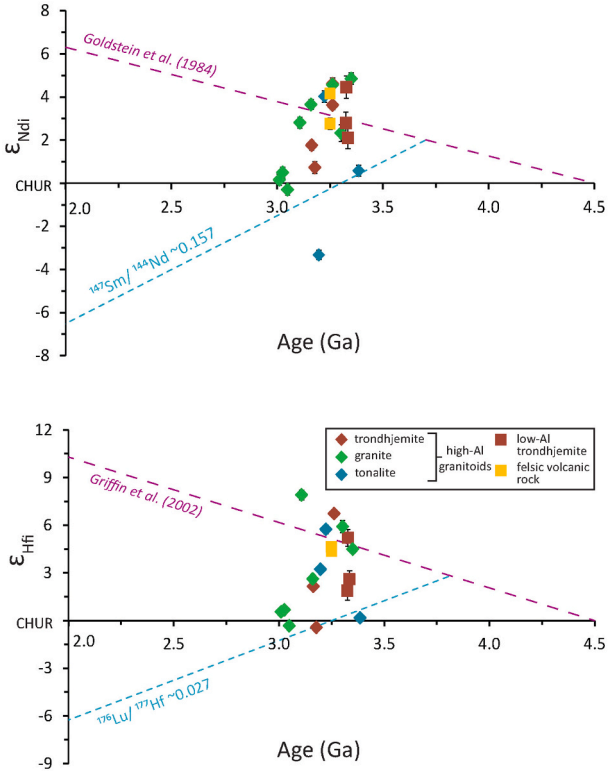

Fig. 7. Whole rock ε_{Hf} vs. age of granitoids and felsic volcanic rocks from the western Dharwar Craton. Ages correspond to concordant U—Pb zircon ages (Table A3; Appendix A). Purple dashed line corresponds to Depleted Mantle lines proposed by Griffin et al. (2002). Slope of blue dashed line corresponds to average $^{176}Lu/^{177}Hf$ of granitoid rocks. CHUR refers to Chondritic Uniform Reservoir. (For interpretation of the references to colour in this figure legend, the reader is referred to the web version of this article.)

within the larger uncertainties of their in-situ measurements. For the rest of the samples, εHf_i of the whole rock and that of the zircon differ considerably, by as much as 1.5 ε-units (Fig. 8a). In that case, only the εHf_i values of zircon are preferred because of slight disturbance of the whole rock isotope systematics possibly during late Archean to Proterozoic overprint (see lower intercepts of zircon in Fig. 5). This selection also depends on the number of zircons measured in-situ and the uncertainties related to their weighted averages.

Rocks with the oldest zircon crystallization ages in the craton have zircon εHf_i ranging from 3.8 ± 1.2 to 8.6 ± 0.9 (Table 3). Rocks with zircon ages younger than 3.25 Ga have less radiogenic Hf isotope compositions and range from $\varepsilon Hf_i = -0.4 \pm 0.7$ to 6.6 ± 0.5. The preferred values from Table 3, after comparison of εHf_i values obtained with three different analytical methods and scrutiny of CL images, are compiled in Fig. 8b and compared with other ε_{Hfi} values reported for granitoid rocks in the western Dharwar Craton.

4.5. Bulk rock Rb—Sr isotope systematics

The calculated initial $^{87}Sr/^{86}Sr$ for the older granitoids range from 0.695558 (low-Al trondhjemite SG 30.2) to 0.702339 (low-Al trondhjemite CHK 38.1), and the initial ratios for the younger granitoids range from 0.695694 (trondhjemite HNL 7.1) to 0.703843 (granite HNL 7.2) (Table A5; Appendix A). The large spread of the initial $^{87}Sr/^{86}Sr$ values and the presence of values lower than the solar system initial (~0.699; Papanastassiou and Wasserburg, 1968) can be attributed to post-emplacement disturbance of the Rb—Sr system, which has a large effect on the calculated initial Sr-isotope ratios. Therefore, the Rb—Sr isotope data collected from bulk rocks of the western Dharwar Craton does not yield robust initial $^{87}Sr/^{86}Sr$ for these rocks.

4.6. Common Pb isotope compositions of leached feldspar

Initial Pb (common Pb) isotope compositions of nine granitoids, three volcanic rocks and two pegmatite samples from the western Dharwar Craton were determined on sequentially leached feldspar grains (Table 4). The Pb isotopes of the feldspar residues, obtained after strong leaching, are shown in Fig. 9 together with the evolution curve for the Bulk Silicate Earth ($\mu = 8.63$, $\kappa = 4.05$; Maltese and Mezger, 2020) and the primitive mantle ($\mu = 8.9$, $\kappa = 4.21$; Kamber and Collerson, 1999).

In both $^{208}Pb/^{204}Pb$ vs. $^{206}Pb/^{204}Pb$ and $^{207}Pb/^{204}Pb$ vs. $^{206}Pb/^{204}Pb$ diagram (Fig. 9), feldspar grains show a large spread attesting to variability in Th/U (κ) and U/Pb (μ) of their host rocks or precursors. All feldspars combined show an evolution history with a wide range of high and low μ and κ; only some of the tonalites and pegmatites being close to mantle values.

5. Discussion

Acknowledging the impact of late metamorphism on early Archean

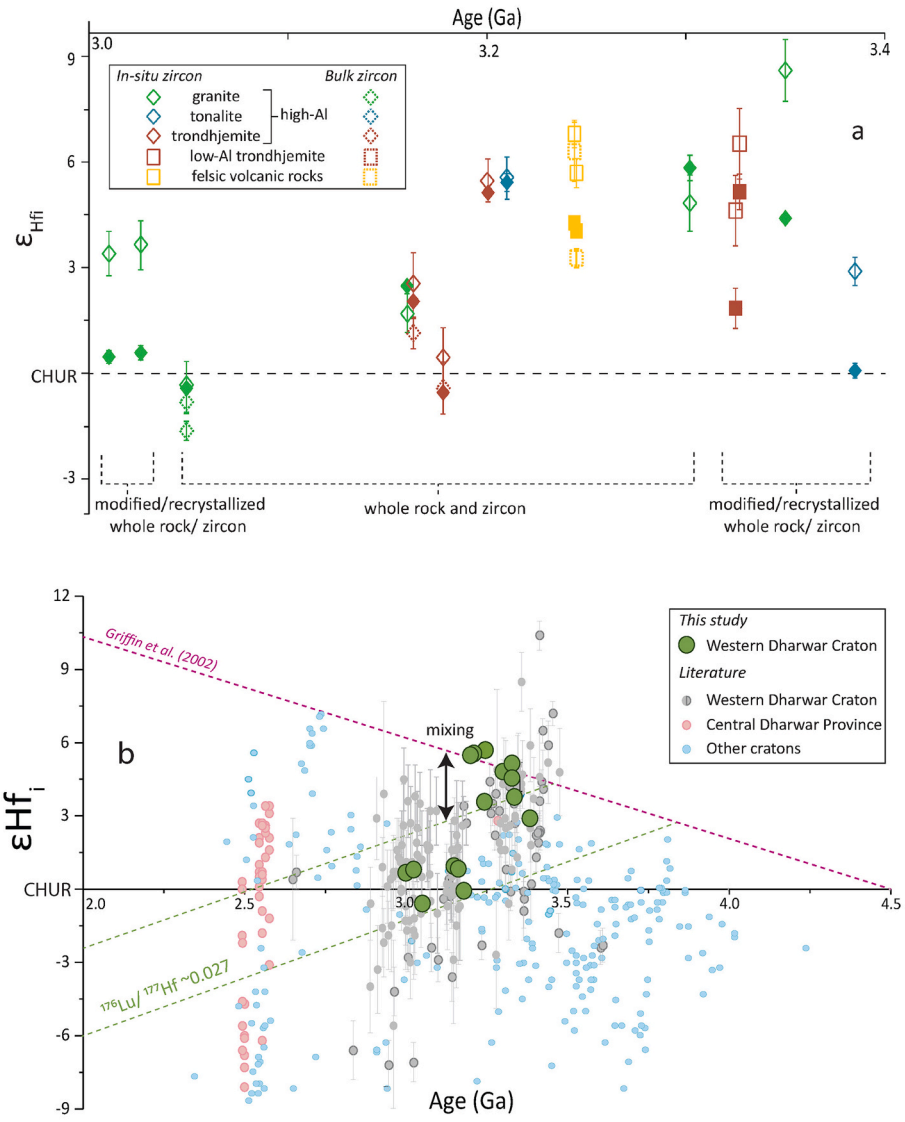

Fig. 8. Initial ε_{Hf} vs. age of granitoid rocks in the western Dharwar Craton. (a) Compiled ε_{Hfi} values of selected granitoid samples obtained in this study by whole rock isotope dilution, in-situ laser on zircon and isotope dilution of bulk single zircon after dissolution. Filled symbols correspond to whole rock ε_{Hfi} values and are the same as in Fig. 7. (b) The best estimates of ε_{Hfi} values from Fig. 8a plotted with other reported ε_{Hfi} values of granitoids from different global Precambrian cratons. Error bars (Tables 2 & 3) are removed for clarity. ε_{Hfi} values of granitoids from the western Dharwar Craton are represented by filled grey circles (Ao et al., 2021) and filled grey circles with darker rims (Guitreau et al., 2017; Ranjan et al., 2020); Central Dharwar Province (Ram Mohan et al., 2014; Yang and Santosh, 2015; Ratheesh-Kumar et al., 2016) by filled pink circles. The light blue circles represent ε_{Hfi} values of felsic rocks from different cratons around the world are compiled from literature (Bauer et al., 2017; Chaudhuri et al., 2018; Dey et al., 2017; Fisher and Vervoort, 2018; Gardiner et al., 2017; Gardiner et al., 2019; Geng et al., 2012; Hiess and Bennett, 2016; Iizuka et al., 2009; Kaur et al., 2014; Kaur et al., 2016; Kaur et al., 2019; Kemp et al., 2009; Kemp et al., 2010; Kröner et al., 2013; Kröner et al., 2014; Kröner et al., 2016; Liu et al., 2009; Laurent and Zeh, 2015; Næraa et al., 2012; Ao et al., 2021; Pandey et al., 2019; Reimink et al., 2016; Saha et al., 2015; Upadhyay et al., 2019; Wan et al., 2014; Wang et al., 2015; Wu et al., 2005; Zeh et al., 2009; Zeh et al., 2011). In most cases, 2 SD <1.5 units with some exceptions (Ao et al., 2021; Iizuka et al., 2009; Bauer et al., 2017; Geng et al., 2012; Wu et al., 2005). (For interpretation of the references to colour in this figure legend, the reader is referred to the web version of this article.)

crustal rocks that can have disturbed their primary geochronological information, several models have been proposed to estimate the amount of continental crust produced during Earth's history from their chemical and isotopic compositions. One extreme model claims that the bulk continental crust present today was produced immediately after the formation of the Earth (Armstrong, 1991). Others have argued for not much crust produced in the Eoarchean to early Paleoarchean (Condie and Aster, 2010; Rino et al., 2004; Taylor and McLennan, 1985). More recent models based on different isotope proxies (Hf—O isotopes in zircon, bulk rock Rb/Sr) have suggested that the net crustal growth was high from ~4.3 to 3.0 Ga and subsequently decreased significantly (Belousova et al., 2010; Dhuime et al., 2012; Dhuime et al., 2015). Due to major differences in these models, the amount and extent of early crust formed remains to be quantified. Therefore, a multi-dimensional detailed study based on geochemical and radio-isotope data of preserved granitoid rocks from the western Dharwar Craton can extend the available information on the possible sources, the timing of melt production and the amount of felsic crust produced, based on new and published isotope data (e.g., Hf- Nd-Pb-Sr) on granitic rocks and individual minerals (e.g., ε_{Hf} from zircon).

5.1. Geochemical constraints on the growth of the western Dharwar Craton

5.1.1. Major and trace element constraints on petrogenesis

Major element characteristics of granitoid rocks in the western Dharwar Craton indicate that the granitoids are chemically highly evolved, of which the TTGs being derived from mafic melts (Fig. 2). In general, the younger granitoids are K-rich compared to the older granitoids. Some of the younger granitic rocks with high K_2O and low Na_2O contents (Fig. 2b & c) fall in the high K-calc alkaline field (Fig.B5; Appendix B). These chemical characteristics of the different granitoids is consistent with the older granitoids, particularly the TTGs, being derived from a mafic source by partial melting and subsequent differentiation, and the younger granitoids being derived from a more incompatible element enriched intermediate to felsic source. Thus the two types of granitoids record an increasing degree of differentiation of the continental crust during its evolution leading towards cratonization (e.g., Sisson et al., 2005). The comparison of major and trace element abundances in granitoids (this study) with those in slightly older basaltic rocks (Ravindran et al., 2021) from the craton confirms that the older granitoids, particularly the members of the TTG suite, were derived from a mafic crustal source by partial melting (Rapp and Watson, 1995; Rapp et al., 2003; Foley et al., 2002).

Table 3
εHf_i of zircon grains in granitoid and felsic volcanic rocks from the western Dharwar Craton.

Sample	Concordant age	In situ zircon		Dissolved zircon	
		εHf_i	±2SD	εHf_i	±2SD
	(Ma)	(average)		(individual)	
GHH 22.3	3010(±25)	+3.4	0.6		
GHH 22.1	3026(±26)	+3.7	0.5		
GHH 22.4	3197(±11)	+7.2	0.5	+4.9	0.4
CHK 36.1	3049(±21)	−0.4	0.7	−0.8	0.3
				−1.6	0.3
SG 43.1	3107(±20)	+6.6	0.5		
SG 31.1	3302(±25)	+4.8	0.6		
SG 30.3	3327(±16)	+6.5	0.6		
SG 30.2	3325(±30)	+4.6	0.3		
SG 34.1	3385(±13)	+2.9	0.4		
SG 32.1	3160(±12)	+1.7	0.4		
HNL 6.3	3200(±18)	+5.4	0.7		
HNL 6.1	3210	+5.6	0.4		
CHK 38.1	3335(±20)	+3.8	1.2		
SG 32.2	3163(±10)	+2.5	0.7	+1.1	0.5
BB 8.2	3244(±9)	+6.8	0.4	+6.3	0.8
BB 8.1	3245(±10)	+5.7	0.4	+3.3	0.3
SG 29.1	3178(±10)	+0.4	0.4	−0.4	0.5
SG 27.1	3350(±11)	+8.6	0.9		

In situ measurements represent the average of a number of analyses of each sample (Table A4; Appendix A). εHf_i of dissolved zircon represent individual grains.

Constraints on the source rocks can be derived from trace element ratios such as Sr/Y and La/Yb that can be tracers of the depth of melting of the source of granitoid rocks (Moyen, 2011). These ratios also function as good qualitative tracers that give relative constraints reflecting the presence or absence of garnet in the source. The formation of trondhjemites (except the low-Al trondhjemites) at high pressures (>15 kbar) is indicated by high Sr/Y, high La/Yb and the absence of significant negative Eu anomalies. Most of the granitoids (TTGs and granites) in the western Dharwar Craton have pronounced negative Ti, Nb and Ta anomalies, which is typical for melting of a mafic source with rutile as a residual phase (Klemme et al., 2002). High $(La/Yb)_N$ of the trondhjemites (except low-Al trondhjemites) and medium to high $(La/Yb)_N$ of the tonalites (Fig. 4 and Table 1) indicate different degrees of melting of a mafic source with different residual phases depending on the depth of partial melting and source composition. Differences in source mineralogy are also indicated by the different Zr/Sm ratios.

The trace element abundances in trondhjemites, except low-Al trondhjemites, and some of the tonalites indicate their formation at high pressure conditions where garnet is stable in the source (Moyen and Martin, 2012). Thus, the combined trace element parameters of these rocks are consistent with melting of an eclogitic source (e.g., Rapp and Watson, 1995; Foley et al., 2002; Klemme et al., 2002) with garnet and rutile as characteristic and significant residual mineral phases. In contrast, the granitoids belonging to the older TTG suite show REE patterns that are less steep than the members of younger TTG suite, which indicates a change in the source rock with time from an older amphibolite residue to a younger eclogite residue for the high-Al parent melts.

Low-Al trondhjemites have major element concentrations similar to those of other trondhjemites in the craton but have distinctive Sr/Y, La/Yb ratios and Nb and Ta abundances. These rocks have been characterized as low-Al TTGs in other studies of the western Dharwar Craton (e.g., Jayananda et al., 2018) and have also been identified in other cratons (Laurent et al., 2019; Zeh et al., 2013). As these rocks are chemically more evolved than the high-Al TTGs and have older emplacement ages (~3.33 Ga), it is less likely that both rock types are formed by the same process or the same source. The low Al2O3, Sr/Y and La/Yb of the low-Al trondhjemites can be attributed to the presence of residual plagioclase in the source (e.g., Jayananda et al., 2018), indicating low pressure conditions during melting of their mafic source. The presence of residual pyroxene could have led to the relative enrichment of HREEs compared to the other granitoids. Pronounced negative Eu and Sr anomalies require significant plagioclase fractionation during their petrogenesis, which also support relatively low pressure conditions. Elevated Nb and Ta compared to other granitoids in the craton might be due to the presence of titanite in the residue, which has lower partition co-efficients for Nb and Ta than rutile (John et al., 2011). Representing some of the oldest, granitoid rocks in the craton, the highly evolved nature of these low-Al trondhjemites can be as a result of higher degrees of partial melting of a slightly older mafic source. Differentiation of the older basaltic material that led to the formation of the other high-Al TTGs in the craton cannot be the process involved in the formation of these highly evolved rocks. For these ~3.33 Ga rocks, melting of a pyroxene-rich source with plagioclase and titanite in the residue indicates a low-pressure partial melting regime of basaltic material at shallow depths. Therefore, the origin of these rocks makes them distinct from the typical Archean TTG suite (Moyen and Martin, 2012).

5.1.2. Zircon U—Pb ages and magmatic episodes

Based on zircon from tonalites, the oldest known granitoids from the western Dharwar Craton formed at ~3.4 Ga and are exposed in the Gorur region. This age agrees with other concordant U—Pb zircon ages reported from different igneous rocks of the same area (e.g., Jayananda et al., 2015; Guitreau et al., 2017).

Single zircon grains from sedimentary rocks were dated in order to evaluate the range in primary ages of source rocks from a large area and to reveal potentially old crustal units that could have gone unrecognized in the record preserved in the igneous bodies. However, deriving a robust, maximum age from detrital zircons is challenging because of the difficulties in ascertaining the right crystallization ages of these grains

Table 4
Common Pb isotope data of leached feldspars present in granitoids and volcanic rocks in western Dharwar Craton.

Sample	$^{206}Pb/^{204}Pb$	±1SE	$^{207}Pb/^{204}Pb$	±1SE	$^{208}Pb/^{204}Pb$	±1SE
BB 8.1	15.9993	0.0005	15.5194	0.0004	34.1812	0.0012
BB 8.2	16.6217	0.0003	15.5486	0.0003	34.1207	0.0007
GHH 21.1	15.5325	0.0008	15.1059	0.0007	34.8540	0.0018
GHH 22.3	13.8364	0.0003	14.7705	0.0003	34.0813	0.0008
SG 32.1	13.4898	0.0006	14.5709	0.0009	35.2299	0.0030
SG 34.1	20.6621	0.0006	18.3308	0.0005	34.1315	0.0010
CHK 36.1	14.0740	0.0002	15.1786	0.0002	35.1250	0.0005
CHK 38.1	15.2282	0.0003	15.1994	0.0003	33.8268	0.0006
GHH 22.2	13.8970	0.0002	14.6796	0.0002	34.0084	0.0005
HNL 6.1	13.6683	0.0007	14.5908	0.0008	33.4177	0.0018
HNL 6.2	13.1608	0.0008	14.5299	0.0010	33.3726	0.0023
HNL 6.3	14.4888	0.0009	14.8401	0.0011	34.0466	0.0024
HNL 7.1	24.8775	0.0016	17.3318	0.0013	34.9415	0.0026
HNL 7.2	13.7804	0.0009	14.7265	0.0011	33.2419	0.0027

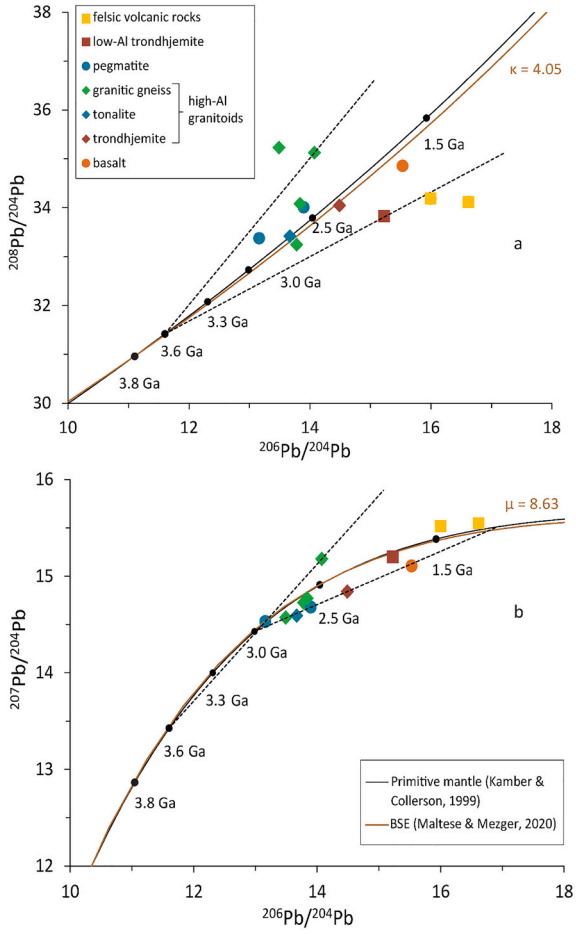

Fig. 9. Pb isotope diagrams (a) $^{208}Pb/^{204}Pb$ vs. $^{206}Pb/^{204}Pb$ (b) $^{207}Pb/^{204}Pb$ vs. $^{206}Pb/^{204}Pb$ showing the initial Pb isotope compositions obtained from leached feldspar grains separated from felsic intrusive (TTGs, granites and pegmatites) and volcanic (basaltic to rhyolitic) rocks in the western Dharwar Craton. The black dashed lines show model evolution trends of initial Pb isotope ratios from 3.6 and 3.0 Ga.

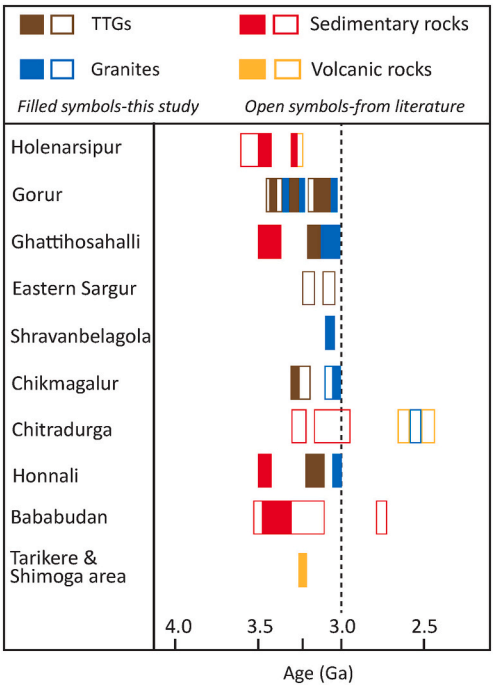

Fig. 10. Compiled zircon U—Pb ages from this study and the literature (Peucat et al., 1993, 1995, 2013; Nutman et al., 1992, 1996; Trendall et al., 1997a, 1997b; Bhaskar Rao et al., 2008; Hokada et al., 2013; Jayananda et al., 2006, 2015; Lancaster et al., 2015; Maibam et al., 2016, 2017; Guitreau et al., 2017; Ranjan et al., 2020; Panicker et al., 2021; Ravindran et al., 2021; Ranjan et al., 2022). The U—Pb ages of TTGs, granites and volcanic rocks correspond to their concordant ages and those of sedimentary rocks correspond to their $^{207}Pb/^{206}Pb$ ages.

that come from various source rocks and may show different extents of disturbance. Detrital and inherited zircons as old as 3.6 Ga are found associated with the Sargur-Holenarsipur area (Nutman et al., 1992; Bhaskar Rao et al., 2008; Lancaster et al., 2015; Guitreau et al., 2017; Ranjan et al., 2022; this study), which could have hosted the oldest crustal basement. Maximum depositional ages as old as 3.45 Ga in the Ghattihosahalli region are reported for the first time through this study. Sedimentary rocks from the younger Bababudan area also have similarly old detrital zircon ages reported by other studies (3.63 Ga; Bhaskar Rao et al., 2008). Quartzites in this area have maximum depositional ages as old as 3.38–3.44 Ga (this study). Sedimentary rocks of the younger Gadag and Shimoga greenstone belts also give indications of crustal relics as old as 3.6–3.5 Ga (Sarma et al., 2012; this study). Fig. 10 presents a detailed compilation of concordant U—Pb ages and $^{207}Pb/^{206}Pb$ ages of granitic, volcanic and sedimentary rocks in the western Dharwar Craton.

Granitoids in the Gorur region formed within a time interval of ~300 Ma, with most of the TTGs emplaced before ~3.1 Ga. Granitoids, mainly TTGs, from the areas adjacent to Ghattihosahalli, Shimoga and Bababudan greenstone belts were emplaced later, at ~3.2 Ga. Rocks emplaced after 3.15 Ga are dominantly granites and they intruded in all these regions. All zircon grains from the major units of the western Dharwar Craton show ages between 3.6 Ga and 3.0 Ga, which further indicates that essentially all felsic continental crust formed during this time period. Emplacement of granitoid rocks lasted for a longer time period in this region than the other regions in the craton and could have involved at least two distinct magmatic-tectonic pulses in the Archean-from 3.40–3.33 Ga and from 3.20–3.15 Ga, as indicated by the clustering of U—Pb ages of magmatic zircon (Fig. 5). Most of the zircon suites in the oldest TTGs from the craton show no evidence of disturbance by thermal overprints until the Cambrian. Granites and low-Al trondhjemites from the craton indicate lower intercept ages that may be related to a thermal disturbance during the pan-African orogeny that affected a major part of southern Indian subcontinent, particularly the Proterozoic regions to the east and south of the Dharwar Craton (e.g., Brandt et al., 2014; Axelsson et al., 2020 and references therein).

5.1.3. *Crust-mantle evolution from Rb—Sr, Pb isotopes*

The Rb—Sr isotope system can potentially give highly resolved information on early crust formation and its subsequent differentiation due to the sensitivity of the Rb/Sr ratio and thus $^{87}Sr/^{86}Sr$ to different fractionation processes in the petrogenesis of continental crust. This sensitivity can also be a major disadvantage due to the susceptibility to post-emplacement metamorphism, which represents a key problem of the Rb—Sr system in terrestrial whole rocks when trying to derive robust initial $^{87}Sr/^{86}Sr$ compositions (e.g., Ravindran et al., 2020). A slight modification of the Rb/Sr following initial crystallization of a magmatic rock can lead to significant changes in the calculated initial isotope ratios due to the fast evolution of the $^{87}Rb—^{87}Sr$. As a consequence, the calculated initial Sr isotope compositions of the granitoids can show an apparent large range for the time given by the U—Pb zircon ages of these rocks. Some of the granitoid rocks in the western Dharwar Craton, which might have undergone late metamorphism at ~ 3.0 and ~ 2.5 Ga (e.g., Jayananda et al., 2013), have their bulk rock Rb/Sr ratio modified leading to higher apparent initial $^{87}Sr/^{86}Sr$ than the primary initial value (Table A4; Appendix A). Some later disturbance of the rocks is also indicated by the generally discordant U—Pb ages of magmatic zircon

leading to post-Archean lower intercepts with concordia (Fig. 5). Therefore, the calculated initial $^{87}Sr/^{86}Sr$ ratios of these granitoids provide only limited constraints on the evolution of their source rocks. However, the overall unradiogenic initial $^{87}Sr/^{86}Sr$ ratios of the different granitoids (Table A5; Appendix A) indicate the absence of Hadean and early Archean enriched material in the source of the granitoids. This observation is also supported by the in-situ Sr-isotope analyses of individual apatite grains extracted from the same rock suite (Fig. 1) (Ravindran et al., 2020). Pristine apatite can be a more suitable phase for obtaining reliable and robust initial Sr-isotope compositions as it has Rb/Sr close to zero. Thus, primary apatite crystals can preserve the Sr isotope composition of their host rock at the time of crystallization making these data more suitable for the reconstruction of the early stages in the petrogenesis of these granitoids as shown in Ravindran et al. (2020).

Similar to the Rb—Sr system, the U-Pb/Pb-Pb system in bulk rocks is highly sensitive to fractionation processes during the petrogenesis of continental crust due to the rapid ingrowth of daughter isotopes as a result of large parent/daughter fractionation. In addition, later thermal overprint, fluid-rock interaction, alteration and weathering can readily fractionate U from Pb on the bulk rock scale. Therefore, obtaining initial Pb isotope compositions of bulk rocks for the time of their magmatic crystallization is difficult due to post-crystallization modification of the U—Pb systematics (e.g., Kamber et al., 2003) and recent U—Pb fractionation due to weathering of the rocks on the surface of the Earth. Minerals such as K-feldspar and galena strongly exclude U and Th, thus showing only minor ingrowth of radiogenic Pb. Particularly K-feldspar, but also to some extent plagioclase can preserve initial Pb isotope compositions which can approximate the Pb isotope compositions of the whole rock sample at the time of last chemical equilibration. However, alteration or inclusions of U-rich mineral can result in radiogenic Pb isotopes that obscure the initial isotope composition. These later additions of radiogenic Pb can be reduced or eliminated by leaching of feldspars that preferentially removes altered material and U-rich inclusions. The residual feldspar after careful examination under a binocular microscope and vigorous leaching in acid should approximate closely the Pb isotope composition of its host at the time of last equilibration. Insufficient leaching of radiogenic Pb can result in too radiogenic Pb isotope compositions of K-feldspar, a problem that was also already observed in studies on the western Dharwar Craton (e.g., Meen et al., 1992).

The measured Pb-isotope compositions of the residual feldspar grains after strong leaching define a rough linear trend in $^{207}Pb/^{204}Pb$ vs. $^{206}Pb/^{204}Pb$ (Fig. 9b) that indicates a later equilibration of the feldspars with their host rocks during Proterozoic time (Bhaskar Rao et al., 1992) or as early as 3.0 Ga (Meen et al., 1992). This thermal overprint is also observed in the U—Pb systematics of some zircon samples (Fig. 5e-h). The combined data array is consistent with an origin of the granitoids or their precursor material from a mantle source prior to 3.0 Ga. The most primitive samples combined suggest derivation of a juvenile crust from a mantle source starting at ca. 3.6 Ga (Fig. 9b), which is consistent with the constraints from Hf isotope systematics and the Sr isotope composition of apatite reported in Ravindran et al. (2020) for the same rock suite. This interpretation is also consistent with $^{208}Pb/^{204}Pb$ vs. $^{206}Pb/^{204}Pb$ systematics of feldspars (Fig. 9a).

The combined $^{206}Pb/^{204}Pb$-$^{207}Pb/^{204}Pb$-$^{208}Pb/^{204}Pb$ isotope data implies significant Th/U/Pb fractionation as early as ca. 3.6 Ga in the petrogenesis and evolution of the granitoids. The rocks contain material derived from a source that had a mantle-like Pb isotope composition until ~3.6 Ga. The material evolved with different U/Th but similar U/Pb until at ~3.4 Ga when the first granitoids were derived from this older material. The regional U—Pb zircon data is consistent with this timeline (Fig. 11). The oldest zircons formed at ~3.6 Ga (e.g., Sarma et al., 2012 and reference therein) and subsequent widespread granitic magmatism lasted from 3.4–3.0 Ga (Fig. 5). The lack of high initial $^{207}Pb/^{204}Pb$ ratios in leached feldspar is consistent with the absence of significant amounts of evolved Hadean or Eoarchean material.

A crustal extraction age of 3.6 Ga is suggested for the western Dharwar Craton, which is the best estimate taken from common Pb (this study) and initial $^{87}Sr/^{86}Sr$ isotope constraints for the same rock suite (Ravindran et al., 2020). Due to the sensitivity of common Pb and Rb—Sr isotopes to crustal extraction compared to Sm—Nd, Lu—Hf isotopes, which was previously used for finding the crustal extraction age of the western Dharwar Craton (e.g., Jayananda et al., 2015; Ranjan et al., 2020), 3.6 Ga can be a more robust estimate for the beginning of the major episode of formation of intermediate to felsic continental crust.

5.1.4. *Crust-mantle evolution from Lu—Hf isotope system*

5.1.4.1. Consistency of whole rock Lu—Hf isotopes. The oldest crustal rocks in the western Dharwar Craton have initial $^{176}Hf/^{177}Hf$ ratios indicating their derivation from a mild to significantly depleted source rock. The younger granitoids in the craton have zero to slightly negative εHf_i values, indicating an origin from a chondritic juvenile source or slightly enriched older mafic source.

In most of the granitoids from the western Dharwar Craton, whole rock εHf_i-εNd_i correlate (Fig. B6; Appendix B), as is expected for rocks that formed by magmatic differentiation ultimately from a mantle source (e.g., Vervoort et al., 2011). This correlation indicates that Lu—Hf isotope compositions preserved in whole rocks can be used as a potentially reliable measure for recovering the initial isotope composition of the samples, and thereby information about the nature of the source of the granitoid rocks in the craton. Initial Hf isotope compositions can be obtained from whole rock samples via back-calculation to the known time of formation, provided the samples have not been disturbed in their Lu/Hf ratio after formation. Due to their low Lu/Hf, initial Hf-isotopes can be measured directly on zircon that formed at the time of magmatic emplacement.

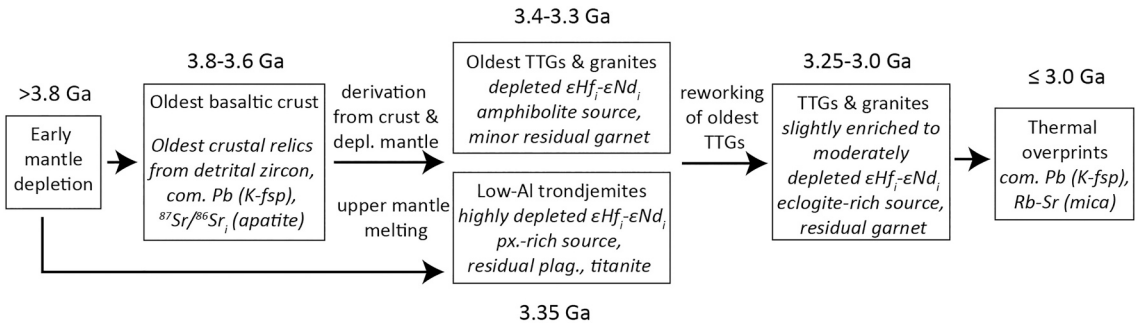

Fig. 11. Timeline showing the episodic growth of continental crust in the western Dharwar Craton. (Abbreviations: K-fsp = K-feldspar, sign. = significantly, plag. = plagioclase, px. = pyroxene, com.Pb = common Pb) (2columns).

5.1.4.2. Significance of Hf isotopes in zircon. Two different methods were used to obtain the Hf-isotope composition of zircon: 1) In-situ measurements of mounted zircon grains using a MC-ICPMS coupled with a laser ablation source and 2) complete dissolution of single grains followed by chromatographic separation of Hf and analysis on a MC-ICPMS. Both methods have advantages and limitations. The advantage of in-situ measurements is that essentially the same spot or two very close spots can be analysed for Hf-isotopes and U—Pb ages, minimizing the ambiguity of assigning the correct age to the Hf isotope composition of a single zircon grain or parts of it. However, as these analyses typically involve two different laser spots (unless measured by split-stream), the initial Hf isotope composition measured from a particular laser spot might correspond to parts of a grain that yields a younger U—Pb age as a result of Pb-loss. This could be a possibility in the case of complex terranes such as the western Dharwar Craton, where zircon grains with multiple overgrowths and significant Pb-loss have been reported (e.g., Jayananda et al., 2015; Ranjan et al., 2020). Also, ancient Pb-loss in zircon grains can, due to the relatively large uncertainty in U/Pb ratio measurements, result in analytically concordant ages that postdate mineral growth and result in assigning the wrong ages for calculating the initial ε_{Hf} value of a specific zircon grain (e.g., Zeh et al., 2014). In addition, the necessary corrections for interferences from Yb on Hf isotopes can compromise the reliability of the in-situ measured $^{176}Hf/^{177}Hf$ isotope compositions (e.g., Fisher et al., 2014). The major disadvantage of the in-situ measurement techniques for Hf isotopes (e.g., Reimink et al., 2019; Ao et al., 2021) is the generally, significantly large uncertainty compared to isotope ratios measured by MC-ICPMS (see Maltese et al., 2021). Initial Hf ratios of magmatic zircon grains from the western Dharwar Craton that have undergone a complex thermal history and measured by in-situ laser technique (e.g., Ao et al., 2021; Guitreau et al., 2017) need to be re-checked to evaluate the robustness of the measured values. This requires an alternative method that can also help constrain the measured values to a single initial Hf isotope ratio per sample instead of the average of measured values.

For meaningful Hf isotope measurements by MC-ICPMS on bulk single zircon grains after chemical purification of Lu and Hf (Maltese et al., 2021), only magmatic zircons grown in one event and having no inclusions, show no evidence of significant Pb-loss and yield concordant U—Pb ages were preferred. Selection of the oldest concordant zircon for bulk Hf-isotope analysis also solves the problem associated with younger overgrowths that result from later magmatic or metamorphic events (e.g., Gerdes and Zeh, 2009). To test the robustness of the selected grain for bulk Hf-isotope analyses, the $^{176}Hf/^{177}Hf$ ratios obtained are compared with the $^{176}Hf/^{177}Hf$ ratios from the respective samples obtained from in-situ measurements on zircons and isotope dilution measurements on bulk whole rock powders. In general, there is good agreement among the measured Hf-isotope composition of zircon from an individual sample using the different analytical methods (Fig. 8a). The tonalite sample (SG 34.1) has three, almost consistent εHf_i measured in-situ from three different zircon grains (Table A4, Appendix A), which confirms the robustness of the chosen data for further interpretation. An exception are the analyses of granitic sample SG 27.1 that show a large range of initial ε_{Hf} values. This spread is due to the presence of abundant inclusions that are visible in the CL images of individual zircon grains. For this reason, this complex sample (SG 27.1) is omitted from further discussion.

The initial ε_{Hf} values of most of the low Al-trondhjemites cluster together within the limits of analytical uncertainty, which indicates that the range of values can be chosen to represent Lu—Hf evolution of crustal rocks emplaced at that specific time (~3.33 Ga). The initial ε_{Hf} values of younger granitic gneisses from the Ghattihosahalli area (GHH 22.1, GHH 22.3) also indicate slight disturbance which could be either due to late metamorphism of the whole rock or inclusions as identified in CL images of their zircon grains (Fig.B2c; Appendix B). These two samples were collected from two different locations that are part of a large outcrop, and therefore, are not expected to be isotopically distinct from each other. The whole rock Lu—Hf isotope compositions show similarities (Table 2) and their εHf_i-εNd_i correlate (Fig.B6; Appendix B). As the initial ε_{Hf} values measured in-situ for these samples represent the average of three analyses each on different zircon grains, the spread (represented as 2 SD_{mean}) can be due to bias in the spots selected for analysis. Due to the consistency of εHf_i values obtained by whole rock isotope dilution measurements of these samples, these values are taken for further interpretation of crustal evolution of the western Dharwar Craton.

Initial ε_{Hf} obtained by using three different methods (whole rocks, in-situ and bulk zircon analysis) confirm the spread of εHf_i of granitoid rocks from other regions of the western Dharwar Craton (Fig. 8b). The εHf_i range between values for the depleted mantle and CHUR. Overall, the εHf_i show a slight trend towards more negative values with time. This isotope array is consistent with an origin of the granitoids from at least two distinct sources and mixing of this material. One source is the depleted mantle and the other, an enriched source like an older mafic crust that had developed an apparent CHUR composition for Hf isotopes. The Hf-isotope systematics are consistent with this older material having been derived from the depleted mantle at ca. 3.8 Ga. An evolution line with $^{176}Lu/^{177}Hf \sim 0.027$ is suggested for these rocks (Fig. 8b), which is consistent with derivation of these granitoids with low εHf_i from a mafic precursor. This interpretation is strongly supported by the results from Sr isotope compositions of whole rocks and apatite that are highly sensitive to Rb/Sr fractionation and indicate enrichment in the source of the granites after ca. 3.8 Ga (Ravindran et al., 2020). The slight trend of more negative εHf_i with time indicates an increasing contribution of older mafic crustal material with time.

In Fig. 8b, εHf_i values of granitoid rocks from the western Dharwar Craton are plotted along with reported εHf_i values of granitoid rocks from the Dharwar Craton and other Precambrian cratons worldwide. This data indicates that the isotope systematics and thus the petrogenesis of granitoids in Paleoarchean cratons appear to have been similar.

5.2. Crust-mantle evolution of the western Dharwar Craton

The western Dharwar craton shows a dome-and-basin structure (e.g., Bouhallier et al., 1995; Chardon et al., 1998) made up of greenstone belts with mostly mafic extrusive rocks and sedimentary rocks surrounded by intrusive granitoids mostly of the TTG suite and late K-rich granites that intruded both units. The craton has undergone significant deformation and metamorphism reaching amphibolite facies conditions, especially in the southern part of the craton, where the oldest crustal rocks are preserved. Hence, a multi-dimensional detailed study using different high-precision analytical techniques based on geochemical and radio-isotope data of preserved granitoid rocks from the western Dharwar Craton is required to reconstruct the origin and evolution of the crust and underlying mantle of the craton. The combination of U—Pb ages with element abundances and Hf, Sr and Pb isotopes from rocks and their components provides constraints on the origin and evolution of continental crust that constitute the present western Dharwar Craton.

The U—Pb ages of magmatic zircons from the western Dharwar Craton indicate that the preserved felsic crust is the product of a multi-stage melting and differentiation history that spans over ~1 Ga with several distinct and resolved major rock-forming intervals dominantly from 3.4–3.0 Ga and some minor magmatic activity until 2.5 Ga (Fig. 10). The chemical and isotope composition of granitoids and sediments in the western Dharwar Craton combined with age constraints from zircon can be integrated to reconstruct a sequence of events and processes that led from the emplacement of mantle-derived material to the formation of evolved felsic continental crust (Fig. 11).

The oldest zircon ages are preserved as detrital mineral grains in sedimentary rocks and formed at ~3.6–3.5 Ga (Lancaster et al., 2015; Maibam et al., 2016; Nutman et al., 1992; Sarma et al., 2012; Ranjan et al., 2022; this study). These rare detrital zircons attest to the formation of the oldest granitoids at that time. Based on the ages of zircons in

magmatic rocks, the oldest extant, felsic intrusive bodies in the western Dharwar Craton are TTGs that crystallized at ~3.40–3.30 Ga (Fig. 11). Major and trace element compositions of these granitoids indicate that they derived from a mafic source dominated by pyroxenite or amphibolite. The chemically distinct low-Al trondhjemites formed by shallow melting of pyroxene-rich material with plagioclase and titanite in the residual melt. This petrogenetic evolution of the granitoids is supported by the combined Hf-Sr-Pb isotope systematics of the rocks and the Hf isotopes of zircon.

The depleted mantle-like Hf isotope compositions of the first TTGs in the craton indicate they formed by differentiation of material derived from a depleted mantle source (Fig. 8b). The TTGs emplaced in the craton at ~3.20 Ga have εHf_i that indicate derivation from an apparently CHUR-like source. However, a derivation from older slightly enriched mafic material derived from the depleted mantle at <3.8 Ga is a more realistic model, as it is also consistent with Sr (Ravindran et al., 2020) and Pb (Fig. 9) isotope systematics. The vertical array of datapoints in the Hf isotope diagrams (Figs. 7, 8) indicates the mixing of material derived from two distinct sources. One being juvenile depleted mantle-derived material and the other older enriched crustal material that originally derived from the depleted mantle significantly earlier and had developed an Hf isotope composition similar to CHUR by the time of granitoid emplacement. This also indicates that melt production from the depleted mantle may have been continuous throughout the time of major continental crust formation in the craton, but addition of reprocessed material to these melts increased with time (Fig. 8b).

The interpretation proposed by this study is consistent with the combined Hf-Sr-Pb systematics of the oldest granitoids in the craton that indicate that their (mafic) source material was derived from the depleted mantle at ~3.8–3.6 Ga (Fig. 11). Evidence for the existence of some enriched (dominantly mafic) crustal material as old as ~3.6 Ga, but not older than 3.8 Ga, is shown by Pb—Sr isotope systematics of these rocks (Fig. 9; Ravindran et al., 2020). Unradiogenic $^{87}Sr/^{86}Sr$ of apatites from granitoids (Ravindran et al., 2020) support the absence of detectable amounts of evolved intermediate to felsic crust older than 3.8 Ga in the craton. The most primitive Pb isotope compositions (Fig. 9) from leached feldspars are also consistent with the absence of significant amounts of evolved, felsic crust, i.e., crust with elevated U/Pb ratios, older than 3.6 Ga being involved in its genesis. These two sensitive isotope systems agree with the Hf isotope systematics recorded in whole rocks and zircon (Figs. 7, 8). As the Hf (and Nd) isotope systems can relate only to an approximate time for depletion of the mantle and need not always correspond to the time when the first crustal material was extracted from the mantle, an agreement with Pb—Sr isotope systematics confirms the interpretation. The combined Hf-Sr-Pb isotopes indicate the formation of a first enriched crust in the Sargur Group and in the Holenarsipur region of the western Dharwar Craton after 3.8 Ga. Subsequent reworking of this mafic material and mixing with juvenile mantle-derived melts in a narrow time interval at 3.4–3.0 Ga generated the different granitoid rocks that dominate the area.

Shallow melting of a pyroxenite/amphibolite source is evident from the trace element abundances (Fig. 3) of the oldest granitoids, which, after ~3.25 Ga, shifted to a much more enriched source and increased melt contribution derived from an eclogitic source. This is confirmed by the transition of major and trace element patterns of granitoids emplaced after 3.25 Ga, indicating deeper melting during their formation with garnet and rutile in the residuum. Shallow melting of upper mantle involved in the formation of the oldest rocks later changed to deeper slab melting under eclogite facies conditions. Specially the rocks that formed after 3.25 Ga preserve element abundances indicating melt formation at a depth where eclogite is stable. This implies an increase in the depth of melt generation over time. The different chemical compositions of the granitoids (TTGs and granitic gneisses) in the craton are, therefore, due to different melting conditions involving mixing of material derived from the depleted mantle and a mafic source that ranged from lower pressure pyroxene-dominated material to a high pressure garnet-rutile-bearing source. Such different melting conditions are possible in different tectonic settings such as modern-day island arcs (e.g., Abouchami et al., 1990; Boher et al., 1992). Alternatively, melting of a mafic source at different pressures is also possible in plume-type setting, where very thick mafic, and most likely hydrated, crust is formed that subsequently melts at different depths (Hernández-Montenegro et al., 2021). The geochemical constraints provided in this study do not permit a unique discrimination between these two end-member models.

After ~3.2 Ga, the decreasing εHf_i values with time and the increasing dominance of granites indicate increasing contributions of reworked evolved crust and decreasing contributions of depleted mantle as crustal growth proceeded in the craton (Fig. 11). This could be due to longer residence time of the older mafic precursor on the surface. The more evolved granites formed at ~3.1–3.0 Ga in different parts of the craton (Fig. 11), which marks the end of a major period of formation of felsic continental crust in the western Dharwar Craton. These late granites derived by direct re-melting of the enriched mafic crust that was generated at ~3.6 Ga but not before 3.8 Ga, and followed by differentiation, as evident from their Pb—Sr isotope systematics (Fig. 9; Ravindran et al., 2020). By ~3.1 Ga, the craton was dominated by evolved continental crust (Fig. 11), which also coincides with the first episode of rapid continental crust formation on a global scale (e.g., Dhuime et al., 2012; Dhuime et al., 2015).

Major felsic crust formation ended in the region at ~3.0 Ga, after which a later magmatic episode at ~2.6 Ga led to the emplacement of the youngest granitic plutons (e.g., Jayananda et al., 2006). Subsequent minor modifications of the rocks in the western Dharwar Craton were caused by later metamorphic overprints that reached greenschist to amphibolite facies conditions at ~2.5 Ga (Jayananda et al., 2013) and coincide with the formation of the adjacent eastern Dharwar Craton and its amalgamation with the western Dharwar Craton. Rubidium-Sr mica ages as young as 2.0 Ga indicate a late low-temperature overprint of the region (Bhaskar Rao et al., 1992; Meen et al., 1992).

6. Conclusions

The origin and evolution of the felsic continental crust of the Western Dharwar Craton is summarized in Fig. 11. The Hf-Sr-Pb isotope systematics of granitoids combined with their chemical compositions provide constraints on the petrogenesis of crustal rocks in the Western Dharwar Craton. Uranium-Pb ages of zircon yield key time-markers for the age of evolved material in the craton and for the emplacement of the different granitoid bodies in the craton. These geochemical signatures reveal that mafic crust in this region did not form before 3.8 Ga. The first felsic crust may have formed by 3.6 Ga as indicated by few U—Pb ages of detrital zircons preserved in sedimentary rocks of the greenstone belts. However, no evidence of preserved rocks from this time has been found so far. Evidence for older enriched material is preserved in the Hf isotope compositions of the granitoids and sedimentary rocks. The felsic rocks date from 3.4 Ga onwards with a major peak of granitoid formation at 3.4–3.0 Ga. This pulse of crust formation coincides temporally with crust formation in other Archean cratons such as the Kaapvaal Craton (e.g., Zeh et al., 2011), the Pilbara Craton (e.g., Kemp et al., 2010), the North China Craton (e.g., Wu et al., 2005), the Bundelkhand Craton (e.g., Kaur et al., 2016) and the Singhbhum Craton (e.g., Upadhyay et al., 2019) and apparently marks the initiation of a rapid continental crust formation in the Archean. The low-Al granitoids emplaced at ca. 3.35 Ga are the closest representatives of the depleted mantle formed by shallow melting of a depleted mantle-derived basaltic/pyroxenitic component. The high-Al granitoids emplaced during this time formed as a result of mixing of a depleted mantle component and an earliest mafic crustal component followed by further magmatic differentiation. After ~3.2 Ga until 3.0 Ga, reworking of the older crust resulted in the emplacement of the younger granitoids in the craton.

The granitoids of the western Dharwar Craton may also record a

change in crustal growth processes. Studies have suggested that after ~3.7 Ga, igneous rocks that build up the continental crust formed by deeper levels of melting in arc-like tectonic environments (e.g., Ranjan et al., 2020; Jayananda et al., 2015). Formation of granitoid rocks after ~3.25 Ga involving melting under high pressure conditions can be related to a subduction regime in the western Dharwar Craton. However, the geodynamic regime that existed at that time cannot be confirmed through radiogenic isotopes and trace element abundances, which can only ascertain the nature of the granitoid sources, but not the tectonic setting. A striking feature of the TTG suite is that the older members formed by shallow melting of a mafic source and the younger members by melting of a deeper source. This change in the melting conditions can be related to a change in the tectonic style and setting that occurred during the time interval of granitoid formation in the Dharwar Craton. The formation of juvenile mafic crust followed by highly evolved crustal material may be related to a change in the tectonic setting, with this change initiating and enabling rapid continental crust formation in the Dharwar Craton and other Paleoarchean cratons.

The western Dharwar Craton is petrologically similar to other cratons of the Indian shield, but there are significant differences. The multi-episodic magmato-tectonic evolution of the Dharwar Craton contrasts with the origin and evolution of the Singhbhum Craton where the continental crust formation was completed by ~3.2 Ga (Pandey et al., 2019; Upadhyay et al., 2019), the Bastar Craton with two significant and well-separated crust formation episodes at ~3.4 Ga and ~ 2.5 Ga (Maltese et al., 2021) and the eastern Dharwar Craton that formed in a short time interval at ~2.5 Ga (Jayananda et al., 2020). Additionally, an intermediate stage involving the formation of basaltic melts by shallow melting of the depleted mantle is absent in the rock record of the western Dharwar Craton. This could be due to rapid evolution of the oldest TTGs and granites from the basaltic precursor rock/melts that completely erased the record of mafic/ultramafic rocks older than ~3.30 Ga in the craton (Ravindran et al., 2021; Jayananda et al., 2008 and references therein). These differences indicate that the first major episode of continental crust formation in the western Dharwar Craton was not uniform, which can be due to a different tectonic setting prevalent at that time. Information on crustal residence times of Archean granitoid rocks in the craton is required to constrain the exact geodynamic regime (e.g., sluggish single-lid, stagnant-lid; Gerya, 2019; Stern, 2018) that operated during the formation of these granitoid rocks that are the major component of the western Dharwar Craton.

Declaration of Competing Interest

None.

Data availability

Data will be made available on request.

Acknowledgements

The research was financially supported by fellowship to AR from ESKAS under the Federation Council of Switzerland (FCS) and the Swiss National Foundation (grant nr. 17452). The Neptune MC-ICP-MS at the Institute of Geological Sciences, University of Bern, Switzerland used in this study was acquired within the framework of the NCCR project PlanetS (grant nr. 51NF40-141881). DU acknowledges financial support from IIT Kharagpur for the setting up of MC-ICPMS laboratory. We are grateful to Sibin Sebastian, Pondicherry University, India, for his assistance with the fieldwork at Karnataka, India. We are thankful to Alessandro Maltese at the Institute of Geological Sciences, University of Bern, Switzerland for his help in the lab for the bulk dissolution of zircons. Detailed and constructive comments provided by Martin Guitreau and Armin Zeh on an earlier version of this manuscript helped to improve the presentation and content. We are also thankful to the Editor Sonja Aulbach and the two reviewers of the manuscript for their constructive and insightful comments.

Appendix A. Supplementary data

Supplementary data to this article can be found online at https://doi.org/10.1016/j.chemgeo.2022.121196.

References

Abouchami, W., Boher, M., Michard, A., Albarede, F., 1990. A major 2.1 Ga event of mafic magmatism in West Africa: an early stage of crustal accretion. J. Geophys. Res. Solid Earth 95, 17605–17629. https://doi.org/10.1029/JB095iB11p17605.

Amelin, Y., Lee, D.C., Halliday, A.N., 2000. Early-middle Archaean crustal evolution deduced from Lu-Hf and U-Pb isotopic studies of single zircon grains. Geochim. Cosmochim. Acta 64, 4205–4225. https://doi.org/10.1016/S0016-7037(00)00493-2.

Ao, W., Zhai, M., Zhao, Y., Zhang, C., Sun, Y., George, P.M., Sajeev, K., Gou, L., Lu, J., Hu, Y., 2021. Paleo-Mesoarchean crustal growth and reworking in the western Dharwar Craton, southwestern India: evidence from trondhjemitic gneiss and granitic gneiss. Precambrian Res. 367, 106428 https://doi.org/10.1016/j.precamres.2021.106428.

Armstrong, R.L., 1991. The persistent myth of crustal growth. Aust. J. Earth Sci. 38, 613–630.

Axelsson, E., Mezger, K., Ewing, T., 2020. The Kuunga Orogeny in the Eastern Ghats Belt: evidence from geochronology of biotite, amphibole and rutile, and implications for the assembly of Gondwana. Precambrian Res. 347, 105805 https://doi.org/10.1016/j.precamres.2020.105805.

Bast, R., Scherer, E.E., Sprung, P., Fischer-Gödde, M., Stracke, A., Mezger, K., 2015. A rapid and efficient ion-exchange chromatography for Lu-Hf, Sm-Nd and Rb-Sr geochronology and the routine isotope analysis of sub-ng amounts of Hf by MC-ICP-MS. J. Anal. At. Spectrom. 30, 2323–2333. https://doi.org/10.1039/C5JA00283D.

Bauer, A.M., Fisher, C.M., Vervoort, J.D., Bowring, S.A., 2017. Coupled zircon Lu–Hf and U–Pb isotopic analyses of the oldest terrestrial crust, the >4.03 Ga Acasta Gneiss Complex. Earth Planet. Sci. Lett. 458, 37–48. https://doi.org/10.1016/j.epsl.2016.10.036.

Belousova, E.A., Kostitsyn, Y.A., Griffin, W.L., Begg, G.C., O'Reilly, S.Y., Pearson, N.J., 2010. The growth of the continental crust: Constraints from zircon Hf-isotope data. Lithos 119, 457–466. https://doi.org/10.1016/j.lithos.2010.07.024.

Bhaskar Rao, Y.J., Sivaraman, T.V., Pantulu, G.V.C., Gopalan, K., Naqvi, S.M., 1992. Rb-Sr ages of late Archaean metavolcanics and granites, Dharwar craton, South India and evidence for early Proterozoic thermotectonic event (s). Precambrian Res. 59, 145–170. https://doi.org/10.1016/0301-9268(92)90055-S.

Bhaskar Rao, Y.J., Kumar, A., Vrevsky, A.B., Srinivasan, R., Anantha Iyer, G.V., 2000. Sm-Nd ages of two meta-anorthosite complexes around Holenarsipur: Constraints on the antiquity of Archaean supracrustal rocks of the Dharwar Craton. J. Earth System Sci. 109, 57–65. https://doi.org/10.1007/BF02719149.

Bhaskar Rao, Y.J., Griffin, W.L., Ketchum, J.W.F., Pearson, N.J., Beyer, E., O'Reilly, S.Y., 2008. An outline of juvenile crust formation and recycling history in the Archaean Western Dharwar Craton, from zircon in situ U-Pb dating and Hf-isotope compositions. Geochim. Cosmochim. Acta 72, A81.

Boher, M., Abouchami, W., Michard, A., Albarede, F., Arndt, N.T., 1992. Crustal growth in West Africa at 2.1 Ga. J. Geophys. Res. Solid Earth 97, 345–369. https://doi.org/10.1029/91JB01640.

Bouhallier, H., Chardon, D., Choukroune, P., 1995. Strain patterns in Archaean dome-and-basin structures: the Dharwar craton (Karnataka, South India). Earth Planet. Sci. Lett. 135, 57–75. https://doi.org/10.1016/0012-821X(95)00144-2.

Bouvier, A., Vervoort, J.D., Patchett, P.J., 2008. The Lu–Hf and Sm–Nd isotopic composition of CHUR: Constraints from unequilibrated chondrites and implications for the bulk composition of terrestrial planets. Earth Planet. Sci. Lett. 273, 48–57. https://doi.org/10.1016/j.epsl.2008.06.010.

Brandt, S., Raith, M.M., Schenk, V., Sengupta, P., Srikantappa, C., Gerdes, A., 2014. Crustal evolution of the Southern Granulite Terrane, South India: New geochronological and geochemical data for felsic orthogneisses and granites. Precambrian Res. 246, 91–122. https://doi.org/10.1016/j.precamres.2014.01.007.

Chardon, D., Choukroune, P., Jayananda, M., 1998. Sinking of the Dharwar Basin (South India): implications for Archaean tectonics. Precambrian Res. 91, 15–39. https://doi.org/10.1016/S0301-9268(98)00037-0.

Chardon, D., Jayananda, M., Peucat, J.J., 2011. Lateral constrictional flow of hot orogenic crust: Insights from the Neoarchean of South India, geological and geophysical implications for orogenic Plateaux. Geochem. Geophys. Geosyst. 12, 1–24. https://doi.org/10.1029/2010GC003398.

Chaudhuri, T., Wan, Y., Mazumder, R., Ma, M., Liu, D., 2018. Evidence of enriched, Hadean mantle reservoir from 4.2-4.0 Ga zircon xenocrysts from Paleoarchean TTGs of the Singhbhum Craton, Eastern India. Sci. Rep. 8, 7069. https://doi.org/10.1038/s41598-018-25494-6.

Chu, N., Taylor, R.N., Nesbitt, R.W., Boella, M., Milton, J.A., German, C.R., Burton, K., 2002. Hf isotope ratio analysis using multi-collector inductively coupled plasma mass spectrometry : an evaluation of isobaric interference corrections. J. Anal. At. Spectrom. 17, 1567–1574. https://doi.org/10.1039/B206707B.

Condie, K.C., Aster, R.C., 2010. Episodic zircon age spectra of orogenic granitoids : the supercontinent connection and continental growth. Precambrian Res. 180, 227–236. https://doi.org/10.1016/j.precamres.2010.03.008.

Couzinié, S., Laurent, O., Moyen, J.-F., Zeh, A., Bouilhol, P., Villaros, A., 2016. Post-collisional magmatism: crustal growth not identified by zircon Hf-O isotopes. Earth Planet. Sci. Lett. 456, 182–195. https://doi.org/10.1016/j.epsl.2016.09.033.
Cowan, G.A., Adler, H.H., 1976. The variability of the natural abundance of 235U. Geochim. Cosmochim. Acta 40, 1487–1490. https://doi.org/10.1016/0016-7037(76)90087-9.
Dey, S., 2013. Evolution of Archaean crust in the Dharwar craton: the Nd isotope record. Precambrian Res. 227, 227–246. https://doi.org/10.1016/j.precamres.2012.05.005.
Dey, S., Topno, A., Liu, Y., Zong, K., 2017. Generation and evolution of Palaeoarchaean continental crust in the central part of the Singhbhum craton, eastern India. Precambrian Res. 298, 268–291. https://doi.org/10.1016/j.precamres.2017.06.009.
Dhuime, B., Hawkesworth, C.J., Cawood, P.A., Storey, C.D., 2012. A change in the geodynamics of continental growth 3 billion years ago. Science 335, 1334–1337.
Dhuime, B., Wuestefeld, A., Hawkesworth, C.J., 2015. Emergence of modern continental crust about 3 billion years ago. Nat. Geosci. 8, 552–555. https://doi.org/10.1038/ngeo2466.
Fisher, C.M., Vervoort, J.D., 2018. Using the magmatic record to constrain the growth of continental crust-the Eoarchean zircon Hf record of Greenland. Earth Planet. Sci. Lett. 488, 79–91. https://doi.org/10.1016/j.epsl.2018.01.031.
Fisher, C.M., Vervoort, J.D., Dufrane, S.A., 2014. Accurate Hf isotope determinations of complex zircons using the "laser ablation split stream" method. Geochem. Geophys. Geosyst. 15, 121–139. https://doi.org/10.1002/2013GC004962.
Fisher, C.M., Bauer, A.M., Vervoort, J.D., 2020. Disturbances in the Sm-Nd isotope system of the Acasta Gneiss Complex-Implications for the Nd isotope record of the early Earth. Earth Planet. Sci. Lett. 530, 115900 https://doi.org/10.1016/j.epsl.2019.115900.
Foley, S., Tiepolo, M., Vannucci, R., 2002. Growth of early continental crust controlled by melting of amphibolite in subduction zones. Nature 417, 837–840. https://doi.org/10.1038/nature00799.
Gardiner, N.J., Hickman, A.H., Kirkland, C.L., Lu, Y., Johnson, T.E., Zhao, J., 2017. Processes of crust formation in the early Earth imaged through Hf isotopes from the East Pilbara Terrane. Precambrian Res. 297, 56–76. https://doi.org/10.1016/j.precamres.2017.05.004.
Gardiner, N.J., Wacey, D., Kirkland, C.L., Johnson, T.E., Jeon, H., 2019. Zircon U–Pb, Lu–Hf and O isotopes from the 3414 Ma Strelley Pool Formation, East Pilbara Terrane, and the Palaeoarchaean emergence of a cryptic cratonic core. Precambrian Res. 321, 64–84. https://doi.org/10.1016/j.precamres.2018.11.023.
Geng, Y., Du, L., Ren, L., 2012. Growth and reworking of the early Precambrian continental crust in the North China Craton: Constraints from zircon Hf isotopes. Gondwana Res. 21, 517–529. https://doi.org/10.1016/j.gr.2011.07.006.
Gerdes, A., Zeh, A., 2009. Zircon formation versus zircon alteration – new insights from combined U-Pb and Lu-Hf in-situ LA-ICP-MS analyses, and consequences for the interpretation of Archean zircon from the Limpopo Belt. Chem. Geol. 261, 230–243. https://doi.org/10.1016/j.chemgeo.2008.03.005.
Gerya, T., 2019. Geodynamics of the early Earth: Quest for the missing paradigm. Geology 47, 1006–1007. https://doi.org/10.1130/focus102019.1.
Griffin, W.L., Wang, X., Jackson, S.E., Pearson, N.J., O'Reilly, S.Y., Xu, X., Zhou, X., 2002. Zircon chemistry and magma mixing, SE China: In-situ analysis of Hf isotopes, Tonglu and Pingtan igneous complexes. Lithos 61, 237–269. https://doi.org/10.1016/S0024-4937(02)00082-8.
Guitreau, M., Blichert-Toft, J., Martin, H., Mojzsis, S.J., Albarède, F., 2012. Hafnium isotope evidence from Archean granitic rocks for deep-mantle origin of continental crust. Earth Planet. Sci. Lett. 337–338, 211–223. https://doi.org/10.1016/j.epsl.2012.05.029.
Guitreau, M., Mukasa, S.B., Loudin, L., Krishnan, S., 2017. New constraints on the early formation of the Western Dharwar Craton (India) from igneous zircon U-Pb and Lu-Hf isotopes. Precambrian Res. 302, 33–49. https://doi.org/10.1016/j.precamres.2017.09.016.
Guitreau, M., Boyet, M., Paquette, J.-L., Gannoun, A., Konc, Z., Benbakkar, M., Suchorski, K., Hénot, J.-M., 2019. Hadean protocrust reworking at the origin of the Archean Napier complex (Antarctica). Geochem. Perspect. Lett. 12, 7–11.
Gupta, S., Rai, S.S., Prakasam, K.S., Srinagesh, D., Priestley, K., Gaur, V.K., 2003. First evidence for anomalous thick crust beneath mid-Archaean western Dharwar craton. Curr. Sci. 84, 1219–1226. https://www.jstor.org/stable/24108425.
Hammerli, J., Kemp, A.I.S., Whitehouse, M.J., 2019. In situ trace element and Sm-Nd isotope analysis of accessory minerals in an Eoarchean tonalitic gneiss from Greenland : Implications for Hf and Nd isotope decoupling in Earth's ancient rocks. Chem. Geol. 524, 394–405. https://doi.org/10.1016/j.chemgeo.2019.06.025.
Hernández-Montenegro, J.D., Palin, R.M., Zuluaga, C.A., Hernández-Uribe, D., 2021. Archean continental crust formed by magma hybridization and voluminous partial melting. Sci. Rep. 11, 5263. https://doi.org/10.1038/s41598-021-84300-y.
Hiess, J., Bennett, V.C., 2016. Chondritic Lu/Hf in the early crust–mantle system as recorded by zircon populations from the oldest Eoarchean rocks of Yilgarn Craton, West Australia and Enderby Land, Antarctica. Chem. Geol. 427, 125–143. https://doi.org/10.1016/j.chemgeo.2016.02.011.
Hokada, T., Horie, K., Satish-kumar, M., Ueno, Y., Nasheeth, A., Mishima, K., Shiraishi, K., 2013. An appraisal of Archaean supracrustal sequences in Chitradurga Schist Belt, western Dharwar Craton. Precambrian Res. 227, 99–119. https://doi.org/10.1016/j.precamres.2012.04.006.
Iizuka, T., Komiya, T., Ueno, Y., Katayama, I., Uehara, Y., Maruyama, S., Hirata, T., Johnson, S.P., Dunkley, D.J., 2007. Geology and zircon geochronology of the Acasta Gneiss complex, northwestern Canada : New constraints on its tectonothermal history. Precambrian Res. 153, 179–208. https://doi.org/10.1016/j.precamres.2006.11.017.
Iizuka, T., Komiya, T., Johnson, S.P., Kon, Y., Maruyama, S., Hirata, T., 2009. Reworking of Hadean crust in the Acasta gneisses, northwestern Canada: evidence from in-situ Lu–Hf isotope analysis of zircon. Chem. Geol. 259, 230–239. https://doi.org/10.1016/j.chemgeo.2008.11.007.
Jackson, S.E., Pearson, N.J., Griffin, W.L., Belousova, E.A., 2004. The application of laser ablation-inductively coupled plasma-mass spectrometry to in situ U–Pb zircon geochronology. Chem. Geol. 211, 47–69. https://doi.org/10.1016/j.chemgeo.2004.06.017.
Jayananda, M., Chardon, D., Peucat, J., Capdevila, R., 2006. 2.61 Ga potassic granites and crustal reworking in the western Dharwar craton, southern India: Tectonic, geochronologic and geochemical constraints. Precambrian Res. 150, 1–26. https://doi.org/10.1016/j.precamres.2006.05.004.
Jayananda, M., Kano, T., Peucat, J., Channabasappa, S., 2008. 3.35 Ga komatiite volcanism in the western Dharwar craton, southern India: Constraints from Nd isotopes and whole-rock geochemistry. Precambrian Res. 162, 160–179.
Jayananda, M., Tsutsumi, Y., Miyazaki, T., Gireesh, R.V., Kapfo, K., Hidaka, H., Kano, T., 2013. Geochronological constraints on Meso- and Neoarchean regional metamorphism and magmatism in the Dharwar craton, southern India. J. Asian Earth Sci. 78, 18–38. https://doi.org/10.1016/j.jseaes.2013.04.033.
Jayananda, M., Chardon, D., Peucat, J., Fanning, C.M., 2015. Paleo- to Mesoarchean TTG accretion and continental growth in the western Dharwar craton, Southern India : Constraints from SHRIMP U–Pb zircon geochronology, whole-rock geochemistry and Nd–Sr isotopes. Precambrian Res. 268, 295–322. https://doi.org/10.1016/j.precamres.2015.07.015.
Jayananda, M., Santosh, M., Aadhiseshan, K.R., 2018. Formation of Archean (3600–2500 Ma) continental crust in the Dharwar Craton, southern India. Earth Sci. Rev. 181, 12–42. https://doi.org/10.1016/j.earscirev.2018.03.013.
Jayananda, M., Aadhiseshan, K.R., Kusiak, M.A., Wilde, S.A., Sekhamo, K.-U., Guitreau, M., Santosh, M., Gireesh, R.V., 2020. Multi-stage crustal growth and Neoarchean geodynamics in the Eastern Dharwar Craton, southern India. Gondwana Res. 78, 228–260. https://doi.org/10.1016/j.gr.2019.09.005.
John, T., Klemd, R., Klemme, S., 2011. Nb–Ta fractionation by partial melting at the titanite–rutile transition. Contrib. Mineral. Petrol. 161, 35–45. https://doi.org/10.1007/s00410-010-0520-4.
Kamber, B., Collerson, K.D., 1999. Origin of ocean island basalts: a new model based on lead and helium isotope systematics. Solid Earth 104, 25479–25491. https://doi.org/10.1029/1999JB000258.
Kamber, B.S., Collerson, K.D., Moorbath, S., Whitehouse, M.J., 2003. Inheritance of early archaean Pb-isotope variability from long-lived hadean protocrust. Contrib. Mineral. Petrol. 145, 25–46. https://doi.org/10.1007/s00410-002-0429-7.
Kaur, P., Zeh, A., Chaudhri, N., 2014. Characterisation and U–Pb–Hf isotope record of the 3.55Ga felsic crust from the Bundelkhand Craton, northern India. Precambrian Res. 255, 236–244. https://doi.org/10.1016/j.precamres.2014.09.019.
Kaur, P., Zeh, A., Chaudhri, N., Eliyas, N., 2016. Unravelling the record of Archaean crustal evolution of the Bundelkhand Craton, northern India using U–Pb zircon–monazite ages, Lu–Hf isotope systematics, and whole-rock geochemistry of granitoids. Precambrian Res. 281, 384–413. https://doi.org/10.1016/j.precamres.2016.06.005.
Kaur, P., Zeh, A., Chaudhri, N., 2019. Archean crustal evolution of the Aravalli Banded Gneissic complex, NW India: Constraints from zircon U-Pb ages, Lu-Hf isotope systematics, and whole-rock geochemistry of granitoids. Precambrian Res. 327, 81–102. https://doi.org/10.1016/j.precamres.2019.03.004.
Kemp, A.I.S., Foster, G.L., Scherstén, A., Whitehouse, M.J., Darling, J., Storey, C., 2009. Concurrent Pb–Hf isotope analysis of zircon by laser ablation multi-collector ICP-MS, with implications for the crustal evolution of Greenland and the Himalayas. Chem. Geol. 261, 244–260. https://doi.org/10.1016/j.chemgeo.2008.06.019.
Kemp, A.I.S., Wilde, S.A., Hawkesworth, C.J., Coath, C.D., Nemchin, A., Pidgeon, R.T., Vervoort, J.D., DuFrane, S.A., 2010. Hadean crustal evolution revisited: New constraints from Pb-Hf isotope systematics of the Jack Hills zircons. Earth Planet. Sci. Lett. 296, 45–56. https://doi.org/10.1016/j.epsl.2010.04.043.
Klemme, S., Blundy, J.D., Wood, B.J., 2002. Experimental constraints on major and trace element partitioning during partial melting of eclogite. Geochim. Cosmochim. Acta 66, 3109–3123. https://doi.org/10.1016/S0016-7037(02)00859-1.
Kooijman, E., Berndt, J., Mezger, K., 2012. U-Pb dating of zircon by laser ablation ICP-MS: recent improvements and new insights. Eur. J. Mineral. 24, 5–21. https://doi.org/10.1127/0935-1221/2012/0024-2170.
Kröner, A., Alexeiev, D.V., Rojas-Agramonte, Y., Hegner, E., Wong, J., Xia, X., Belousova, E., Mikolaichuk, A.V., Seltmann, R., Liu, D., Kiselev, V.V., 2013. Mesoproterozoic (Grenville-age) terranes in the Kyrgyz North Tianshan: Zircon ages and Nd–Hf isotopic constraints on the origin and evolution of basement blocks in the southern Central Asian Orogen. Gondwana Res. 23, 272–295. https://doi.org/10.1016/j.gr.2012.05.004.
Kröner, A., Hoffmann, J.E., Xie, H., Münker, C., Hegner, E., Wan, Y., Hofmann, A., Liu, D., Yang, J., 2014. Generation of early Archaean grey gneisses through melting of older crust in the eastern Kaapvaal craton, southern Africa. Precambrian Res. 255, 823–846. https://doi.org/10.1016/j.precamres.2014.07.017.
Kröner, A., Anhaeusser, C.R., Hoffmann, J.E., Wong, J., Geng, H., Hegner, E., Xie, H., Yang, J., Liu, D., 2016. Chronology of the oldest supracrustal sequences in the Palaeoarchaean Barberton Greenstone Belt, South Africa and Swaziland. Precambrian Res. 279, 123–143. https://doi.org/10.1016/j.precamres.2016.04.007.
Kumar, A., Bhaskar Rao, Y.J., Sivaraman, T.V., Gopalan, K., 1996. Sm-Nd ages of Archaean metavolcanics of the Dharwar craton, South India. Precambrian Res. 80, 205–216.
Lahaye, Y., Arndt, N., Byerly, G., Chauvel, C., Fourcade, S., Gruau, G., 1995. The influence of alteration on the trace-element and Nd isotopic compositions of komatiites. Chem. Geol. 126, 43–64. https://doi.org/10.1016/0009-2541(95)00102-1.

Lancaster, P.J., Dey, S., Storey, C.D., Mitra, A., Bhunia, R.K., 2015. Contrasting crustal evolution processes in the Dharwar craton : Insights from detrital zircon U – Pb and Hf isotopes. Gondwana Res. 28, 1361–1372. https://doi.org/10.1016/j.gr.2014.10.010.

Laurent, O., Zeh, A., 2015. A linear Hf isotope-age array despite different granitoid sources and complex Archean geodynamics: an example from the Pietersburg block (South Africa). Earth Planet. Sci. Lett. 430, 326–338. https://doi.org/10.1016/j.epsl.2015.08.028.

Laurent, O., Zeh, A., Brandl, G., Vezinet, A., Wilson, A.H., 2019. Granitoids and greenstone belts of the Pietersburg block-witnesses of an Archean accretionary orogen along the northern edge of the Kaapvaal Craton. In: The Archaean Geology of the Kaapvaal Craton, Southern Africa. Springer Nature, Switzerland, pp. 83–108. https://doi.org/10.1007/978-3-319-78652-0_4.

Liu, F.L., Gerdes, A., Xue, H.M., 2009. Differential subduction and exhumation of crustal slices in the Sulu HP-UHP metamorphic terrane: insights from mineral inclusions, trace elements, U-Pb and Lu-Hf isotope analyses of zircon in orthogneiss. J. Metamorphic Petrol. 27, 805–825. https://doi.org/10.1111/j.1525-1314.2009.00833.x.

Ludwig, K.R., 2003. User's Manual for ISOPLOT 3.00: A Geochronological Toolkit for Microsoft Excel, Special Publication No. 4. Berkeley Geochronology Center, pp. 1–70.

Maibam, B., Gerdes, A., Goswami, J.N., 2016. U–Pb and Hf isotope records in detrital and magmatic zircon from eastern and western Dharwar craton, southern India : Evidence for coeval Archaean crustal evolution. Precambrian Res. 275, 496–512. https://doi.org/10.1016/j.precamres.2016.01.009.

Maibam, B., Gerdes, A., Srinivasan, R., Goswami, J.N., 2017. U–Pb and Lu–Hf systematics of zircons from Sargur metasediments, Dharwar Craton, Southern India: New insights on the provenance and crustal evolution. Curr. Sci. 113, 1394–1402. https://www.jstor.org/stable/26493043.

Maltese, A., Mezger, K., 2020. The Pb isotope evolution of Bulk Silicate Earth : Constraints from its accretion and early differentiation history. Geochim. Cosmochim. Acta 271, 179–193. https://doi.org/10.1016/j.gca.2019.12.021.

Maltese, A., Mezger, K., Upadhyay, D., Berndt, J., Scherer, E.E., 2021. On the petrogenesis of Paleoarchean continental crust: U-Pb-Hf isotope and major-trace element constraints from the Bastar Craton, India. Chem. Geol. 579, 120337 https://doi.org/10.1016/j.chemgeo.2021.120337.

Maya, J.M., Bhutani, R., Balakrishnan, S., Rajee Sandhya, S., 2017. Petrogenesis of 3.15 Ga old Banasandra komatiites from the Dharwar craton, India: Implications for early mantle heterogeneity. Geosci. Front. 8, 467–481. https://doi.org/10.1016/j.gsf.2016.03.007.

McDonough, W.F., Sun, S.-S., 1995. The composition of the Earth. Chem. Geol. 120, 223–253.

Meen, J.K., Rogers, J.J.W., Fullagar, P.D., 1992. Lead isotopic compositions of the Western Dharwar craton, southern India: evidence for distinct Middle Archaean terranes in a late Archaean craton. Geochim. Cosmochim. Acta 56, 2455–2470. https://doi.org/10.1016/0016-7037(92)90202-T.

Mezger, K., Krogstad, E.J., 1997. Interpretation of discordant U-Pb zircon ages: an evaluation. J. Metamorphic Petrol. 15, 127–140. https://doi.org/10.1111/j.1525-1314.1997.00008.x.

Monrad, J.R., 1983. Evolution of sialic terranes in the vicinity of the Holenarsipur belt, Hassan District, Karnataka, India. In: Precambrian of South India, 4. Geological Society of India, pp. 343–364.

Moorbath, S., Whitehouse, M.J., Kamber, B., 1997. Extreme Nd-isotope heterogeneity in the early Archaean-fact or fiction? Case histories from northern Canada and West Greenland. Chem. Geol. 135, 213–231. https://doi.org/10.1016/S0009-2541(96)00117-9.

Moyen, J.F., 2011. The composite Archaean grey gneisses: Petrological significance, and evidence for a non-unique tectonic setting for Archaean crustal growth. Lithos 123, 21–36. https://doi.org/10.1016/j.lithos.2010.09.015.

Moyen, J.F., Martin, H., 2012. Forty years of TTG research. Lithos 148, 312–336. https://doi.org/10.1016/j.lithos.2012.06.010.

Næraa, T., Scherstén, A., Rosing, M., Kemp, A.I.S., Hoffmann, J.E., Kokfelt, T.F., Whitehouse, M.J., 2012. Hafnium isotope evidence for a transition in the dynamics of continental growth 3.2 Gyr ago. Nature 485, 627–630. https://doi.org/10.1038/nature11140.

Naqvi, S.M., Mohan, M.R., Prathap, J.G.R., Sarma, D.S., 2009. Adakite-TTG connection and fate of Mesoarchaean basaltic crust of Holenarsipur Nucleus, Dharwar Craton, India. J. Asian Earth Sci. 35, 416–434. https://doi.org/10.1016/j.jseaes.2009.02.005.

Nemchin, A.A., Pidgeon, R.T., Whitehouse, M.J., 2006. Re-evaluation of the origin and evolution of >4.2 Ga zircons from the Jack Hills metasedimentary rocks. Earth Planet. Sci. Lett. 244, 218–233. https://doi.org/10.1016/j.epsl.2006.01.054.

Nutman, A.P., Chadwick, B., Ramakrishnan, M., Viswanatha, M.N., 1992. SHRIMP U-Pb ages of detrital zircon in Sargur supracrustal rocks in western Karnataka, southern India. J. Geol. Soc. India 39 (5), 367–374.

Nutman, A.P., Chadwick, B., Krishna Rao, B., Vasudev, V.N., 1996. SHRIMP U-Pb zircon ages of acid volcanic rocks in the Chitradurga and Sandur groups, and granites adjacent to the Sandur Schist Belt, Karnataka. J. Geol. Soc. India 47, 153–164.

Pandey, O.P., Mezger, K., Ranjan, S., Upadhyay, D., Villa, I.M., Nägler, T.F., Vollstaedt, H., 2019. Genesis of the Singhbhum Craton, eastern India; implications for Archean crust-mantle evolution of the Earth. Chem. Geol. 512, 85–106. https://doi.org/10.1016/j.chemgeo.2019.02.040.

Panicker, A.G., Ram Mohan, M., Upadhyay, D., Raju, B.V., Chauhan, H., Chalapathi Rao, N.V., 2021. U-Pb zircon age, geochemistry and petrogenesis of Mesoarchean anorthositic rocks from the Holenarsipur greenstone belt, western Dharwar Craton: Implications for accretionary tectonics in southern India. Lithos 398-399, 106268. https://doi.org/10.1016/j.lithos.2021.106268.

Papanastassiou, D.A., Wasserburg, G.J., 1968. Initial strontium isotopic abundances and the resolution of small time differences in the formation of planetary objects. Earth Planet. Sci. Lett. 5, 361–376. https://doi.org/10.1016/S0012-821X(68)80066-4.

Patchett, P.J., Tatsumoto, M., 1981. A routine high-precision method for Lu-Hf isotope geochemistry and chronology. Contrib. Mineral. Petrol. 75, 263–267. https://doi.org/10.1007/BF01166766.

Peucat, J.J., Mahabaleswar, B., Jayananda, M., 1993. Age of younger tonalitic magmatism and granulitic metamorphism in the South Indian transition zone (Krishnagiri area); comparison with older Peninsular gneisses from the Gorur–Hassan area. J. Metamorphic Petrol. 11, 879–888. https://doi.org/10.1111/j.1525-1314.1993.tb00197.x.

Peucat, J.J., Bouhallier, H., Fanning, C.M., Jayananda, M., 1995. Age of the Holenarsipur Greenstone Belt, relationships with the surrounding gneisses (Karnataka, South India). J. Geol. 103, 701–710. https://doi.org/10.1086/629789.

Peucat, J.J., Jayananda, M., Chardon, D., Capdevila, R., Fanning, C.M., Paquette, J.L., 2013. The lower crust of the Dharwar Craton, Southern India: Patchwork of Archean granulitic domains. Precambrian Res. 227, 4–28. https://doi.org/10.1016/j.precamres.2012.06.009.

Raczek, I., Jochum, K.P., Hofmann, A.W., 2003. Neodymium and strontium isotope data for USGS reference materials BCR-1, BCR-2, BHVO-2, AGV-1, AGV-2, GSP-1, GSP-2 and eight MPI-DING reference glasses. Geostand. Geoanal. Res. 27, 173–179. https://doi.org/10.1111/j.1751-908X.2003.tb00644.x.

Ram Mohan, M., Srinivasa Sarma, D., McNaughton, N.J., Fletcher, I.R., Wilde, S.A., Siddiqui, M.A., Rasmussen, B., Krapez, B., Gregory, C.J., Kamo, S.L., 2014. SHRIMP zircon and titanite U-Pb ages, Lu-Hf isotope signatures and geochemical constraints for ~2.56 Ga granitic magmatism in Western Dharwar Craton, Southern India: evidence for short-lived Neoarchean episodic crustal growth? Precambrian Res. 243, 197–220. https://doi.org/10.1016/j.precamres.2013.12.017.

Ranjan, S., Upadhyay, D., Abhinay, K., Srikantappa, C., 2020. Paleoarchean and Neoarchean Tonalite–Trondhjemite–Granodiorite (TTG) and granite magmatism in the Western Dharwar Craton, southern India: Implications for Archean continental growth and geodynamics. Precambrian Res. 340, 105630 https://doi.org/10.1016/j.precamres.2020.105630.

Ranjan, S., Upadhyay, D., Srikantappa, C., 2022. Eoarchean to Neoarchean crustal evolution of the Western Dharwar Craton, southern India: Clues from U-Pb-Hf isotope composition of detrital zircon. Precambrian Res. 371, 106559 https://doi.org/10.1016/j.precamres.2022.106559.

Rapp, R., Watson, E.B., 1995. Dehydration Melting of Metabasalt at 8–32 kbar: Implications for Continental Growth and Crust-Mantle Recycling. J. Petrol. 36, 891–931. https://doi.org/10.1093/petrology/36.4.891.

Rapp, R., Shimizu, N., Norman, M., 2003. Growth of early continental crust by partial melting of eclogite. Nature 425, 605–609. https://doi.org/10.1038/nature02031.

Ratheesh-Kumar, R.T., Santosh, M., Yang, Q., Ishwar-Kumar, C., Chen, N., Sajeev, K., 2016. Archean tectonics and crustal evolution of the Biligiri Rangan Block, southern India. Precambrian Res. 275, 406–428. https://doi.org/10.1016/j.precamres.2016.01.022.

Ravindran, A., Mezger, K., Balakrishnan, S., Kooijman, E., Schmitt, M., Berndt, J., 2020. Initial $^{87}Sr/^{86}Sr$ as a sensitive tracer of Archaean crust-mantle evolution : Constraints from igneous and sedimentary rocks in the western Dharwar Craton. Precambrian Res. 337, 105523 https://doi.org/10.1016/j.precamres.2019.105523.

Ravindran, A., Mezger, K., Balakrishnan, S., Berndt, J., 2021. Hf-Nd isotopes from ultramafic and mafic rocks in the western Dharwar Craton, India, record early Archean mantle heterogeneity. Lithos 404–405, 106491. https://doi.org/10.1016/j.lithos.2021.106491.

Rehkämper, M., Mezger, K., 2000. Investigation of matrix effects for Pb isotope ratio measurements by multiple collector ICP-MS: verification and application of optimized analytical protocols. J. Anal. At. Spectrom. 15, 1451–1460.

Reimink, Jesse R., Chacko, T., Stern, R.A., Heaman, L.M., 2014. Earth's earliest evolved crust generated in an Iceland-like setting. Nat. Geosci. 7, 529–533. https://doi.org/10.1038/ngeo2170.

Reimink, J.R., Davies, J.H.F.L., Chacko, T., Stern, R.A., Heaman, L.M., Sarkar, C., Pearson, D.G., 2016. No evidence for Hadean continental crust within Earth's oldest evolved rock unit. Nat. Geosci. 9, 777–780. https://doi.org/10.1038/ngeo2786.

Reimink, J.R., Pearson, D.G., Shirey, S.B., Carlson, R.W., Ketchum, J.W.F., 2019. Onset of new, progressive crustal growth in the central Slave craton at 3.55 Ga. Geochem. Perspect. Lett. 10, 8–13.

Reimink, Jesse R., Davies, J.H.F.L., Bauer, A.M., Chacko, T., 2020. A comparison between zircons from the Acasta Gneiss complex and the Jack Hills region. Earth Planet. Sci. Lett. 531, 115975 https://doi.org/10.1016/j.epsl.2019.115975.

Rino, S., Komiya, T., Windley, B.F., Katayama, I., Motoki, A., Hirata, T., 2004. Major episodic increases of continental crustal growth determined from zircon ages of river sands; implications for mantle overturns in the early Precambrian. Phys. Earth Planet. Inter. 146, 369–394. https://doi.org/10.1016/j.pepi.2003.09.024.

Saha, L., Frei, F., Gerdes, A., Pati, J.K., Sarkar, S., Patole, V., Bhandari, A., Nasipuri, P., 2015. Crustal geodynamics from the Archaean Bundelkhand Craton, India: constraints from zircon U–Pb–Hf isotope studies. Geol. Mag. 153, 179–192. https://doi.org/10.1017/S0016756815000692.

Sarma, D.S., Mcnaughton, N.J., Belusova, E., Mohan, M.R., Fletcher, I.R., 2012. Detrital zircon U–Pb ages and Hf-isotope systematics from the Gadag Greenstone Belt: Archean crustal growth in the western Dharwar Craton, India. Gondwana Res. 22, 843–854. https://doi.org/10.1016/j.gr.2012.04.001.

Scherer, E., Münker, C., Mezger, K., 2001. Calibration of the Lutetium-Hafnium clock. Science 29, 683–687.

Sisson, T.W., Ratajeski, K., Hankins, W.B., Glazner, A.F., 2005. Voluminous granitic magmas from common basaltic sources. Contrib. Mineral. Petrol. 148, 635–661. https://doi.org/10.1007/s00410-004-0632-9.

Smit, M., Mezger, K., 2017. Earth's early O2 cycle suppressed by primitive continents. Nat. Geosci. 10, 788–792. https://doi.org/10.1038/ngeo3030.

Stern, R.J., 2018. The evolution of plate tectonics. Phil. Trans. R. Soc. A 376, 1–12. https://doi.org/10.1098/rsta.2017.0406.

Stracke, A., Scherer, E.E., Reynolds, B.C., 2014. Application of isotope dilution in geochemistry. Treatise on Geochemistry (Second Edition), 15. Elsevier, pp. 71–86.

Sun, S.-S., McDonough, W.F., 1989. Chemical and isotopic systematics of oceanic basalts: Implications for mantle composition and processes. Geol. Soc. Lond. Spec. Publ. 42, 323–345.

Swami Nath, J., Ramakrishnan, M., 1981. Early Precambrian supracrustals of southern Karnataka. Geol. Surv. India 112, 350.

Taylor, S.R., McLennan, S.M., 1985. The Continental Crust: Its Composition and Evolution. Blackwell Scientific Publications, Oxford, p. 312.

Taylor, P.N., Chadwick, B., Moorbath, S.M., Ramakrishnan, M., Viswanatha, M.N., 1984. Petrography, chemistry and isotopic ages of Peninsular Gneiss, Dharwar acid volcanic rocks and the Chitradurga Granite with special reference to the late Archaean evolution of the Karnataka Craton, southern India. Precambrian Res. 23, 349–375.

Thirlwall, M.F., Anczkiewicz, R., 2004. Multidynamic isotope ratio analysis using MC–ICP–MS and the causes of secular drift in Hf, Nd and Pb isotope ratios. Int. J. Mass Spectrom. 235, 59–81. https://doi.org/10.1016/j.ijms.2004.04.002.

Trendall, A.F., de Laeter, J.R., Nelson, D.R., Mukhopadhyay, D., 1997a. A precise U–Pb age for the base of Mulaingiri formation (Bababudan Group, Dharwar Supergroup) of the Karnataka craton. J. Geol. Soc. India 50, 161–170.

Trendall, A.F., de Laeter, J.R., Nelson, D.R., Bhaskar Rao, Y.J., 1997b. Further zircon UI-Pb age data for the Daginkatte Formation, Dharwar Supergroup, Karnataka Craton. J. Geol. Soc. India 50, 25–30.

Upadhyay, D., Chattopadhyay, S., Mezger, K., 2019. Formation of Paleoarchean-Mesoarchean Na-rich (TTG) and K-rich granitoid crust of the Singhbhum craton, eastern India: Constraints from major and trace element geochemistry and Sr-Nd-Hf isotope composition. Precambrian Res. 327, 255–272. https://doi.org/10.1016/j.precamres.2019.04.009.

Vervoort, J.D., Kemp, A.I.S., 2016. Clarifying the zircon Hf isotope record of crust-mantle evolution. Chem. Geol. 425, 65–75. https://doi.org/10.1016/j.chemgeo.2016.01.023.

Vervoort, J.D., Plank, T., Prytulak, J., 2011. The Hf–Nd isotopic composition of marine sediments. Geochim. Cosmochim. Acta 75, 5903–5926. https://doi.org/10.1016/j.gca.2011.07.046.

Villa, I.M., Hanchar, J.M., 2013. K-feldspar hygrochronology. Geochim. Cosmochim. Acta 101, 24–33. https://doi.org/10.1016/j.gca.2012.09.047.

Wan, Y., Dong, D., Wang, S., Kröner, A., Xie, H., Ma, M., Zhou, H., Xie, S., Liu, D., 2014. Middle Neoarchean magmatism in western Shandong, North China Craton: SHRIMP zircon dating and LA-ICP-MS Hf isotope analysis. Precambrian Res. 255, 865–884. https://doi.org/10.1016/j.precamres.2014.07.016.

Wang, Y., Zhao, C., Zhang, F., Liu, J., Wang, J., Peng, R., Liu, B., 2015. SIMS zircon U–Pb and molybdenite Re–Os geochronology, Hf isotope, and whole-rock geochemistry of the Wunugetushan porphyry Cu–Mo deposit and granitoids in NE China and their geological significance. Gondwana Res. 28, 1228–1245. https://doi.org/10.1016/j.gr.2014.10.001.

Wiedenbeck, M., Allé, P., Corfu, F., Griffin, W.L., Meier, M., Oberli, F., Von Quadt, A., Roddick, J.C., Spiegel, W., 1995. Three natural zircon standards for U-Th-Pb, Lu-Hf, trace element and REE analyses. Geostand. Geoanal. Res. 19, 1–23. https://doi.org/10.1111/j.1751-908X.1995.tb00147.x.

Wu, F., Yang, J., Liu, X., Li, T., Xie, L., Yang, Y., 2005. Hf isotopes of the 3.8 Ga zircons in eastern Hebei Province, China: Implications for early crustal evolution of the North China Craton. Chin. Sci. Bull. 50, 2473–2480. https://doi.org/10.1360/982005-629Yang.

Yang, Q., Santosh, M., 2015. Zircon U–Pb geochronology and Lu–Hf isotopes from the Kolar greenstone belt, Dharwar Craton, India: Implications for crustal evolution in an ocean-trench-continent transect. J. Asian Earth Sci. 113, 797–811. https://doi.org/10.1016/j.jseaes.2015.05.023.

Zeh, A., Gerdes, A., Barton Jr., J.M., 2009. Archean Accretion and Crustal Evolution of the Kalahari Craton—the Zircon Age and Hf Isotope Record of Granitic Rocks from Barberton/Swaziland to the Francistown Arc. J. Petrol. 50, 933–966. https://doi.org/10.1093/petrology/egp027.

Zeh, A., Gerdes, A., Millonig, L., 2011. Hafnium isotope record of the Ancient Gneiss complex, Swaziland, southern Africa: evidence for Archaean crust–mantle formation and crust reworking between 3.66 and 2.73 Ga. J. Geol. Soc. 168, 953–964. https://doi.org/10.1144/0016-76492010-117.

Zeh, A., Jaguin, J., Poujol, M., Boulvais, P., Hallot, E., Block, S., Paquette, J.-L., 2013. Juvenile crust formation in the northeastern Kaapvaal Craton at 2.97 Ga—Implications for Archean terrane accretion, and the source of the Pietersburg gold. Precambrian Res. 233, 20–43. https://doi.org/10.1016/j.precamres.2013.04.013.

Zeh, A., Stern, R., Gerdes, A., 2014. The oldest zircons of Africa—Their U–Pb–Hf–O isotope and trace element systematics, and implications for Hadean to Archean crust–mantle evolution. Precambrian Res. 241, 203–230. https://doi.org/10.1016/j.precamres.2013.11.006.